Elias Assmann, BSc

Quantum Monte Carlo Simulation of the Attractive Hubbard Model in a Harmonic Confining Potential

MASTER THESIS

For obtaining the academic degree
Diplom-Ingenieur

Master Programme of
Technical Physics

Graz University of Technology

Supervisor:
Ao.Univ.-Prof. Dipl.-Phys. Dr.rer.nat. Hans Gerd Evertz
Institute of Theoretical and Computational Physics

Graz, May 2011

Für Rita, Sophie und Felix, in Liebe.

Abstract

The low-temperature properties of the two-dimensional attractive Hubbard model strongly depend on the fermion density. This fact has fundamental consequences for experiments on ultra-cold atoms in optical lattices, where the magneto-optical trap, which is required experimentally, introduces an inhomogeneous confining potential, which in turn leads to an inhomogeneous particle density ρ_i. In the homogeneous (untrapped) case, away from half-filling, i.e.. at $\rho \neq 1$, there is a Kosterlitz-Thouless transition at a critical temperature $T_c > 0$ to a superfluid phase exhibiting quasi-long-range pair order (QLRO). However, at half-filling pair order is degenerate with charge-density-wave order for symmetry reasons; therefore, the QLRO is suppressed and the system orders only at $T = 0$, where it enters a phase exhibiting long-range order simultaneously in the pairing and charge-density-wave channels.

In this work, the two-dimensional attractive Hubbard model in a harmonic confining potential is studied using determinant quantum Monte Carlo. At low temperatures, we find large pair correlations; a comparison with the so-called local-density approximation shows that the latter makes drastically wrong predictions for the pairing and charge-density-wave correlation functions around half-filling. This means that a larger portion of the system than expected will be superfluid, but also that the physics of the half-filled attractive model is represented anywhere in the trap. Furthermore, in a finite-size extrapolation adapted to the confined case, we show evidence that a Kosterlitz-Thouless transition to a superfluid QLRO phase also occurs in the inhomogeneous case. The transition temperature is roughly estimated to be $T_c \sim 0.15\,t$.

Zusammenfassung

Die Niedertemperatureigenschaften des zweidimensionalen attraktiven Hubbard-Modells hängen wesentlich von der Teilchendichte ab. Dies hat grundlegende Auswirkungen auf Experimente an ultrakalten Atomen in optischen Gittern, denn dort wird durch die experimentell notwendige magneto-optische Falle ein ortsabhängiges Potential eingeführt, weswegen die Teilchendichte ρ_i ebenso ortsabhängig wird. Im homogenen Fall gibt es abseits von Halbfüllung, also bei $\rho \neq 1$, bei einer Sprungtemperatur $T_c > 0$ einen Kosterlitz-Thouless-Übergang zu einer suprafluiden Phase mit quasi-langreichweitiger Paar-Ordnung (QLRO). Bei Halbfüllung ist die Paarbildung jedoch aus Symmetriegründen entartet mit einer Ladungsdichtewelle, wodurch die QLRO unterdrückt wird und erst bei $T = 0$ Ordnung auftritt, nämlich langreichweitige Ordnung der Paar- wie der Ladungsdichtewellen-Korrelationen.

In dieser Arbeit wird das zweidimensionale attraktive Hubbard-Modell mit harmonischem Fallenpotential mittels Determinanten-Quanten-Monte-Carlo untersucht. Bei tiefen Temperaturen treten starke Paar-Korrelationen auf; im Vergleich mit der sogenannten Lokalen-Dichte-Näherung zeigt sich, dass diese im Bereich um Halbfüllung drastisch falsche Voraussagen für die Paar- und Ladungsdichtewelle-Korrelationen macht. Das bedeutet, dass ein größerer Teil des Systems suprafluid wird als angenommen, aber auch dass die Physik des halbgefüllten Modells in der Falle nicht repräsentiert ist. Weiters werden mittels eines geeigneten Vergleichs verschiedener Systemgrößen *(finite-size extrapolation)* Hinweise gezeigt, dass auch im inhomogenen Fall ein Kosterlitz-Thouless Übergang zu einer suprafluiden QLRO-Phase vorliegt. Die Sprungtemperatur wird grob auf $T_c \sim 0.15\,t$ geschätzt.

Acknowledgements

I was fortunate to have Hans Gerd Evertz, Richard Scalettar and Simone Chiesa as my advisors and collaborators. It's been a pleasure working with you and learning from you, and I did learn a great deal. Thank you.

Richard Scalettar provided QUEST, the DQMC code I used for the numerical work, and guided my research at UC Davis. Simone Chiesa, who wrote the QUEST subprogram for trapped systems, was an invaluable help in modifying it for my needs. Simone also implemented the imaginary Hubbard-Stratonovich transformation.

Hans Gerd Evertz was a very supportive advisor and a great mentor. Thank you for an interesting thesis project, for arranging the visit to Davis and helping to secure funding for it, for help and guidance in writing the thesis and preparing presentations, for flexibility in adapting to my time schedule (on more than one occasion), and for everything else. Hans Gerd also provided the second DQMC code that was used for comparison.

The people in the Scalettar group during my time at UC Davis and their families contributed much to making our time in California a pleasurable one. In particular, Richard Scalettar, Dave and Lisa Cone, Simone and Tiziana Chiesa, Brian and Tiffany Neal, and George Batrouni. Thank you for making me feel a bit at home so far from home.

Back home, work on my thesis could not have been nearly so enjoyable (though far be it from me to pretend it was never tedious!) without the kind people at the ITP and the Many-Body Group in particular. To name a few: Martin Ganahl, Valentin Zauner, Michael Knap, and Anna Fulterer. You made this a great place to work without pay.

My family has been incredibly patient and understanding to me. It may seem like a cliché, but in a very real sense, this thesis could not have come into being without support from my wife that went above and beyond what could reasonably be asked for throughout these often trying times.

Generous funding for my stay at UC Davis was received from the Austrian Marshall Plan Foundation. Thank you for your support and your patience.

Finally, no thanks go to: The California DMV, expensive hospitals and bureaucratic health insurance, US visa regulations, unhelpful real-estate agents, and luggage-losing airlines.

Contents

List of Figures

1 Introduction

The motivation for this work stems from optical lattices. An optical lattice is a "crystal of light" formed by the intensity pattern of two or more interfering laser beams. When the lasers are tuned to the right frequency, the optical lattice is able to trap atoms in its nodes or antinodes, as the case may be. The oscillating field induces a dipole moment in the atom which interacts with the field, resulting in an attraction of the atom to either the nodes or the antinodes of the standing wave. In this way, the intensity pattern is analogous to a crystal lattice and the trapped atoms are analogous to the electrons in the crystal.

In recent years, experiments on ultra-cold atoms trapped in optical lattices have attracted much attention from both the experimental and the theoretical side. Experimentally, they represent the confluence of two previously distinct fields of atomic physics, quantum gases and optical lattices, which was sparked by an influential paper published in 1998 by Jaksch et al., suggesting that a superfluid to Mott insulator transition of bosons could be observed in such a system [9, 29]. The authors argued that the system could be tuned in such a way that the atoms would be described by the Bose-Hubbard model. This idea was subsequently realized by Greiner et al. [21].

More recently, experimentalists have been able to trap *fermionic* atoms in optical lattices [32]. At this point contact is made with the forefront of another, more distantly related, discipline: condensed-matter theory. This is because the system becomes a *quantum simulator* of the Fermi-Hubbard model, a model that represents a long-standing problem of that field. The optical lattice can be viewed as a "special-purpose quantum computer"* for simulating the Hubbard model [36].

The Hubbard model is of continued interest as a fundamental, simple model which can nonetheless capture the essence of many phenomena,

*Quantum computing in a more general sense is another field where applications for quantum gases in optical lattices are expected.

and which has been solved exactly only in one dimension. More recently, the model is regarded as a candidate for describing high-temperature superconductivity.

The appeal of the quantum-simulator idea is that these systems are known to follow the Hubbard model to a good approximation; have highly tunable parameters including the hopping amplitude, the strength and sign (repulsive or attractive) of the interaction, the lattice geometry, disorder and impurities in the lattice, and even the dimensionality; and act on much larger time and length scales than real crystals, making novel kinds of observations possible.

The hope in this line of research is to experimentally determine the low-temperature phase diagram of the Hubbard model, which has so far been impossible by theoretical means. Perhaps the most important open question is whether the repulsive Fermi-Hubbard model supports superconductivity and may be able to describe high-temperature superconductors. However, this question is very challenging to address in optical-lattice experiments, primarily because of the extremely low temperatures that are needed. Temperatures achieved in experiments are in the nano-Kelvin range, but the energy scales of the model – the hopping amplitude t and the interaction energy U – are so small that even lower temperatures will be required to reach the parameter regime of interest.

There is an interesting parallel between optical-lattice experiments and quantum Monte Carlo simulations, which are the prime theoretical tool for investigating Hubbard models. In both cases, bosons are easier to study than fermions, and attractive interactions easier than repulsive interactions. Experimentally, this is because of the different temperature-scales involved, theoretically, it is a result of the fermion sign problem.

Thus, until the challenges of the repulsive case are overcome, it is interesting to study fermion superconductivity in the "attractive" Hubbard model, in which fermions on the same lattice site are taken to attract each other. More precisely, in the attractive case one studies superfluidity as an analog of superconductivity. Superfluidity in the attractive case is more confidently expected to exist than superconductivity in the repulsive case.

Theoretical studies alongside the experiments are essential for the quantum-simulator program for the following reasons. First, it is challenging to set up the experiments and make measurements, and guidance from theoretical results is valuable. Second, it is not as straightforwardly

clear that the system follows the Hubbard model as we have made it seem. There are subtleties that have to be kept in check, and agreement with the model has to be verified.

Third, there is a more fundamental difference between atoms in an optical lattice and the traditional Hubbard model. The atoms have to be prevented from exiting the lattice, which is experimentally achieved by a magneto-optical trap; one speaks of a *confined system*. The trap leads to a form of inhomogeneity in the model which was never considered in condensed-matter physics. The immediate physical effect is that the fermion density varies across the system.

In the theory of confined systems, one defines a *local-density approximation*, whereby one attempts to deduce the properties of the trapped system from the homogeneous case. This is of great interest both technically, because it simplifies the calculations, and conceptually, because ultimately one wants to draw conclusions about the homogeneous model from observations of the confined one.

In this work, we will assume the validity of the Hubbard model as a given, and study superfluidity in the confined attractive Fermi-Hubbard model on a two-dimensional square lattice, using determinant quantum Monte Carlo for the numerical calculations. The effects of the trap compared to the conventional homogeneous model and the validity of the local-density approximation will be our main focus.

2 The Hubbard Model

The *Hubbard model* [19, 27, 37] is one of the simplest models of electrons in a crystal, or more generally, of interacting particles on a lattice. In its standard single-band form, it includes the kinetic energy in the form of nearest-neighbor hopping t as in the tight-binding model; and a local density-density interaction U between particles occupying the same site. It is the interplay between these non-commuting terms that gives rise to interesting physics in the model.

The Hubbard model may be obtained from the ab initio Hamiltonian describing a crystal by a series of approximations. It exhibits a variety of phenomena that occur in solid-state systems, for instance Mott insulating behavior and the antiferromagnetic (AF) ordering that accompanies it. Another notable case is high-temperature superconductivity, specifically the cuprate superconductors. It is believed that the CuO_2 layers that form in these materials are central to the superconductivity [52]; since the inter-layer coupling is weak, the layers are regarded as quasi-two-dimensional sheets. The square-lattice Hubbard model is conjectured to describe superconductivity in these sheets, with each site representing a copper atom [1].

While the focus of this work is on a different realization of Hubbard-type models, namely ultra-cold atoms loaded in optical lattices (see Chapter 3), in this chapter the Hubbard model is motivated and discussed from a condensed-matter perspective. Two *particle-hole transformations* are defined which relate different sets of parameters of the model, and which will serve as guidelines to the discussion of the attractive Hubbard model (AHM) throughout the present thesis. Using these transformations, some of the phases occuring in the model are briefly discussed. Finally, relations needed for a finite-size scaling analysis of the superfluid phase are given.

2.1 Hamiltonian

Starting from an ab initio description of nuclei and electrons in a crystal, assuming the nuclei with their core electrons fixed at the equilibrium positions (the Born-Oppenheimer approximation), taking the Wannier functions as single-particle basis, and keeping only a single band, one may derive a Hamiltonian of the form

$$\hat{\mathcal{H}} = -\sum_{ij\sigma} t_{ij}\, c^+_{\sigma i} c_{\sigma j} + \sum_{(i,\sigma)\neq(j,\rho)} U_{ij}\, \hat{n}_{\sigma i}\hat{n}_{\rho j}$$

with hopping amplitudes t_{ij} and interactions U_{ij}. Here and in the following, the indices i and j sum over all lattice sites while σ and ρ sum over spin states. The symbol $\langle ij\rangle$ will be used to denote a pair of nearest-neighbor sites. Using standard second quantized notation, $c^+_{\sigma i}$ is the creation operator for a site i and spin σ, $c_{\sigma i}$ the destruction operator and $\hat{n}_{\sigma i} := c^+_{\sigma i} c_{\sigma i}$ the number operator, while $\hat{n}_i := \hat{n}_{\uparrow i} + \hat{n}_{\downarrow i}$ counts the total number of particles on site i.

The standard Hubbard Hamiltonian follows if we assume that the overlap between basis functions at different sites is sufficiently small (for electrons in a crystal, this means that they are well localized and screened) to consider only local interactions U_{ii} and nearest-neighbor hoppings $t_{\langle ij\rangle}$, and furthermore assume homogeneous interactions $U_{ii} = U$ and hoppings $t_{\langle ij\rangle} = t$. Often, the hopping is used as unit of energy by setting, symbolically, "$t = 1$". Adding a *chemical potential* μ and a *magnetic field** h, the most general form of homogeneous Hubbard model used in this work may be written as

$$\begin{aligned}\hat{H}(t, U, \mu, h) := -t \sum_{\langle ij\rangle\,\sigma} c^+_{\sigma i} c_{\sigma j} + U \sum_i (\hat{n}_{\uparrow i} - 1/2)(\hat{n}_{\downarrow i} - 1/2) \\ - \mu \sum_i (\hat{n}_{\uparrow i} + \hat{n}_{\downarrow i}) - h \sum_i (\hat{n}_{\uparrow i} - \hat{n}_{\downarrow i}). \quad (2.1)\end{aligned}$$

This is the *particle-hole symmetric* form of the Hamiltonian, which behaves

*To fully treat the effect of a magnetic field on charged, spinful particles in non-relativistic quantum mechanics, two changes to the Hamiltonian are needed. First, the Lorentz force is included by substituting $\hat{\mathbf{p}} \mapsto (\hat{\mathbf{p}} - \hat{\mathbf{A}})$ for the momentum, where $\hat{\mathbf{A}}$ is the operator representing the electromagnetic vector potential. In a lattice model, this leads to a *Peierls phase* [46] in the hoppings t_{ij}, but this effect is neglected here.

in a particularly simple manner under the particle-hole transformations discussed in Sec. 2.3. This form is tailored to spin-1/2 fermions. To describe bosons (*Bose-Hubbard model*, BHM), one uses the form

$$\frac{1}{2}U\sum_i \hat{n}_i(\hat{n}_i - 1)$$

for the interaction, where the factor $(\hat{n}-1)/2$ ensures that *pairs* of particles are counted (we have assumed spin-0 bosons here). Note that for spin-1/2 particles $\hat{n}(\hat{n}-1)/2 = \hat{n}_\uparrow\hat{n}_\downarrow$, which is easily shown using the identities $\hat{n} = \hat{n}_\uparrow + \hat{n}_\downarrow$ and $\hat{n}_\sigma^2 = \hat{n}_\sigma$; thus if we re-interpret the operators in the "boson form" of the interaction as spin-1/2 operators, we have

$$U\sum_i \hat{n}_{\uparrow i}\hat{n}_{\downarrow i}$$

for the interaction, a form that is often used for fermions.

In any case, the sign of the interaction U may be positive, leading to a repulsion between the particles (*repulsive Hubbard model*, RHM); or negative, leading to an attraction (*attractive Hubbard model*, AHM). In this work, we will focus on the AHM but discuss certain properties thereof with the help of a relation to the RHM derived in Sec. 2.3. The chemical potential and magnetic field together will be useful in deriving this relationship; the chemical potential is also used to set the particle number in the grand canonical ensemble, which we will be using.

While the formalism will accommodate any lattice geometry in any dimensionality (as encoded by $\langle ij\rangle$), we will stick to a two-dimensional square lattice in this work (this lattice will be referred to as "2D" for short). This case is important for the study of high-temperature superconductivity, as the CuO_2-layers in the cuprate superconductors, which are thought to be responsible for superconductivity in these materials [52], are often modeled by this lattice; it is also often realized in optical-lattice experiments.

Second, the aligning effect on the spin of the particle is accounted for by a Zeeman term $\mathbf{B}\cdot\hat{\mathbf{s}}$ which for the case of a field in z-direction is equivalent to the term $h(\hat{n}_\uparrow - \hat{n}_\downarrow)$ included in (2.1). It is in this restricted sense that we will use the term "magnetic field".

2.2 Observables

In the following, we will assume a bipartite lattice, and use the symbol $(-1)^i$ to mean -1 if i belongs to one sublattice and $+1$ for the other sublattice.

The observables which will be the focus of this work are the *charge correlation function*

$$c_{\text{charge}}(i,j) := \langle \hat{n}_i \hat{n}_j \rangle - \langle \hat{n}_i \rangle \langle \hat{n}_j \rangle, \tag{2.2a}$$

and the *s-wave pairing correlation function*

$$c_{\text{pair}}(i,j) := \langle \Delta_i^+ \Delta_j + \Delta_j^+ \Delta_i \rangle \tag{2.2b}$$

where $\Delta_i^+ := c_{\uparrow i}^+ c_{\downarrow i}^+$ creates a pair of fermions on site i.

We also define the associated *structure factors*, which are used to distinguish the phases of the 2D AHM discussed in Sec. 2.4,

$$S_{\text{CDW}} := \sum_{ij} (-1)^{i+j} \, c_{\text{charge}}(i,j). \tag{2.3a}$$

$$P_s := \sum_{ij} c_{\text{pair}}(i,j), \tag{2.3b}$$

2.3 Particle-Hole Transformations

Combining the creation and destruction operators into vectors $\boldsymbol{c}$ and $\boldsymbol{c}^+$, we can write a standard change of basis as $\boldsymbol{c} \mapsto \boldsymbol{V}\boldsymbol{c}$ and $\boldsymbol{c}^+ \mapsto \boldsymbol{c}^+\boldsymbol{V}^+$, with a unitary matrix $\boldsymbol{V}$. To study the Hubbard model, another type of transformation is useful: *particle-hole transformations*, which map creation operators to destruction operators and vice versa.

Through the action on the fermion operators, these transformations act on all quantum mechanical operators, as written in second quantized notation. The behavior of the Hamiltonian is particularly relevant, but all other observables must change, too. Each transformation ph is self-inverse, $\text{ph} \circ \text{ph} = \text{Id}$ and commutes with the Hermitian conjugate, $\text{ph}(\widehat{A}^+) = (\text{ph}\,\widehat{A})^+$. All the relations in this section follow easily by substitution and using the canonical anticommutation relations of the fermion operators,

$\{c_{\sigma i},\, c^{+}_{\rho j}\} = \delta_{ij}\delta_{\sigma\rho}$ and $\{c_{\sigma i},\, c_{\rho j}\} = \{c^{+}_{\sigma i},\, c^{+}_{\rho j}\} = 0$ where δ is the Kronecker symbol.

2.3.1 Symmetric Particle-Hole Transformation

The creation operator for each site and spin is exchanged with the corresponding destruction operator. An additional factor $(-1)^i$ is needed to keep the hopping term invariant.

$$\mathrm{ph}_{\uparrow\downarrow}: \quad c_{\sigma i} \leftrightarrow (-1)^i c^{+}_{\sigma i} \tag{2.4a}$$

The number and pair-creation evidently operators transform as

$$\begin{aligned} \widehat{n}_{\sigma i} &\leftrightarrow 1 - \widehat{n}_{\sigma i}\,, \\ \Delta^{+}_{i} &\leftrightarrow 1 - \Delta_i\,, \end{aligned} \tag{2.4b}$$

which leaves the hopping and the interaction unchanged but changes the sign of the chemical potential and magnetic field, because of the transformation of the $\widehat{n}_{\sigma i}$

$$\widehat{H}(t, U, \mu, h) \leftrightarrow \widehat{H}(t, U, -\mu, -h). \tag{2.4c}$$

For the observables, one finds

$$\begin{aligned} c_{\mathrm{charge}}(i,j) &\leftrightarrow c_{\mathrm{charge}}(i,j), \\ c_{\mathrm{pair}}(i,j) &\leftrightarrow c_{\mathrm{pair}}(i,j) + 2\delta_{ij}(1 - \widehat{n}_i). \end{aligned} \tag{2.4d}$$

Thus we see, for example, that the particle density obeys the relation $\rho(t, U, \mu, h) = \langle \widehat{n}_i \rangle_{(t,U,\mu,h)} = \langle 2 - \widehat{n}_i \rangle_{(t,U,-\mu,-h)} = 2 - \rho(t, U, -\mu, -h)$ for any set of parameters.

At $\mu = h = 0$, the Hamiltonian is invariant under $\mathrm{ph}_{\uparrow\downarrow}$, and all observables are equal in the particle picture and the hole picture; the model is said to be *particle-hole symmetric* in this case. From the behavior of the density under $\mathrm{ph}_{\uparrow\downarrow}$, we see that $\mu = 0$ corresponds to half-filling, $\rho(\mu = 0) = 1$.

Another consequence is that for fixed t, U, and h, the phase diagram is symmetric about $\mu = 0$. For the CDW and s-wave phases corresponding to the quantities (2.3), this is easily seen from (2.4d), since under $\mathrm{ph}_{\uparrow\downarrow}$, the structure factor S_{CDW} is completely unchanged and P_s is unchanged except for local contributions.

2.3.2 Asymmetric Particle-Hole Transformation

If we swap the creation and destruction operators of only one spin species [16],

$$\begin{aligned} \mathrm{ph}_\downarrow : \quad & c_{\downarrow i} \leftrightarrow (-1)^i c^+_{\downarrow i} \\ & c_{\uparrow i} \text{ unchanged,} \end{aligned} \tag{2.5a}$$

density operators are transformed to spin operators and vice-versa

$$\begin{aligned} \widehat{n}_i &\leftrightarrow 2\widehat{s}_{zi} + 1, \\ \Delta^+_i &\leftrightarrow (-1)^i \widehat{s}^+_i; \end{aligned} \tag{2.5b}$$

and the interaction is seen to change sign, yielding a relation between the attractive and the repulsive Hubbard model

$$\widehat{H}(t, U, \mu, h) \leftrightarrow \widehat{H}(t, -U, \mu, h). \tag{2.5c}$$

Using well-known properties of the spin-$1/2$ operators, the relations for the observables may be derived,

$$\begin{aligned} c_{\mathrm{charge}}(i,j) &\leftrightarrow 4\big[\langle \widehat{s}_{zi}\, \widehat{s}_{zj}\rangle - \langle \widehat{s}_{zi}\rangle\langle \widehat{s}_{zj}\rangle\big], \\ c_{\mathrm{pair}}(i,j) &\leftrightarrow 2\big[(-1)^{i+j}\, \langle \widehat{s}_{xi}\, \widehat{s}_{xj} + \widehat{s}_{yi}\, \widehat{s}_{yj}\rangle + \delta_{ij}\langle \widehat{s}_{zi}\rangle\big]. \end{aligned} \tag{2.5d}$$

Both correlation functions defined in (2.2) are thus mapped to *spin* correlation functions.

2.4 Phases of the 2D AHM

In this section, we will discuss some of the phases that occur in the 2D Hubbard model. While our focus is the attractive model at $h = 0$, we will make heavy use of the relation to the repulsive case at $\mu = 0$ given by (2.5).

2.4.1 At $\mu = 0 \leftrightarrow h = 0$

We begin our discussion with the RHM at $h = \mu = 0$, which maps to the AHM with $\mu = h = 0$. At zero magnetic field, the Hubbard model has

the SU(2) symmetry of spin rotations, even though that symmetry is not manifest in (2.1).* Therefore, all spin components are equivalent

$$\langle \hat{s}_{xi}\, \hat{s}_{xj}\rangle = \langle \hat{s}_{yi}\, \hat{s}_{yj}\rangle = \langle \hat{s}_{zi}\, \hat{s}_{zj}\rangle \qquad (h = 0). \tag{2.6}$$

A finite-temperature phase transition in these circumstances is forbidden in 2D by the Mermin-Wagner theorem [41], but long-range AF spin ordering occurs at zero temperature [56].

As we have seen in (2.5d), spin correlation in the z-direction in the RHM maps to CDW correlation in the AHM, and xy-spin order maps to s-wave pairing, thus (2.6) translates to

$$c_{\text{charge}} \sim c_{\text{pair}} \qquad (\mu = 0), \tag{2.7}$$

up to constants and local contributions. It follows that the half-filled AHM exhibits combined CDW and pair order at $T = 0$, but is unordered at $T > 0$.

To conclude, at $\mu = 0 \leftrightarrow h = 0$ the 2D Hubbard model in is unordered at finite temperature, but at $T = 0$, it possesses true *long-range order*, where the appropriate correlation functions decay to constants at large distances,

$$c(r) \to \text{const} > 0 \qquad \text{for } r \to \infty. \tag{2.8}$$

Here, c stands for a generic correlation function such as $c(|\vec{r}_i - \vec{r}_j|) := \langle \hat{s}_i\, \hat{s}_j\rangle$ and is not to be confused with a fermion destruction operator. In the repulsive case, it is the spin degrees of freedom that order, and the three spin directions are degenerate. In the attractive case, CDW and pair order occur simultaneously [51]. Spin and CDW ordering is depicted schematically in Fig. 2.1.

2.4.2 At $\mu \neq 0 \leftrightarrow h \neq 0$

Going to nonzero magnetic field $h \neq 0$ but staying at half-filling $\mu = 0$ (in the repulsive picture), the spin symmetry is broken, and the z-component singled out, which makes possible a Kosterlitz-Thouless (KT) transition

*The SU(2) symmetry can be made manifest by writing $\hat{H}$ in terms of spinors $\psi^+ = \begin{pmatrix} c_\uparrow^+ & c_\downarrow^+ \end{pmatrix}$ and the z-Pauli matrix $\sigma_z = \left(\begin{smallmatrix} 1 & 0 \\ 0 & -1 \end{smallmatrix}\right)$. It then reads $\hat{H} = -t\sum_{\langle ij\rangle} \psi_i^+\psi_j + U\sum_i (\psi_i^+\psi_i)^2 - \mu\sum_i \psi_i^+\psi_i - h\sum_i \psi^+\sigma_z\psi$, up to a shift in chemical potential [18].

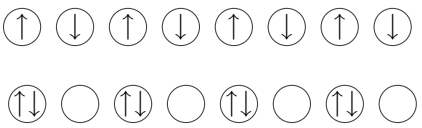

Figure 2.1: Schematic illustration of phases in the 2D Hubbard model. Top: antiferromagnetic spin order as it occurs in the RHM with $\mu = h = 0$ at $T = 0$. Bottom: charge-density wave order as it occurs simultaneously with s-wave pairing order in the AHM with $\mu = h = 0$ at $T = 0$.

[34] to a phase with quasi-long-range order (QLRO) in the xy-spin degrees of freedom at a finite critical temperature T_c.

In the RHM, the low-temperature phase again exhibits antiferromagnetic correlations, but only with regard to the xy-components of the spin; in the AHM, it is the pairing that is preserved, while the CDW disappears.

In either case, it is no longer true long-range order that occurs, but QLRO meaning that the correlations decay to zero as a power of the distance, $c(r) \sim r^{-(d-2+\eta)}$ in d dimensions or, in two dimensions,

$$c(r) \sim r^{-\eta} \qquad \text{for } r \to \infty \quad (T < T_c). \tag{2.9a}$$

Above the transition temperature, a finite correlation length ξ enters,

$$c(r) \sim r^{-\eta}\, e^{-r/\xi} \qquad \text{for } r \to \infty \quad (T > T_c). \tag{2.9b}$$

The critical exponent η is known at zero temperature, $\eta(T = 0) = 0$ [7] and at the transition temperature $\eta(T_c) = 1/4$ [33]. It is seen that in the ground state, the QLRO becomes true long-range order in 2D.

2.5 Finite-Size Scaling for the KT Transition

In a finite-size scaling analysis (FSS) [44], systems of different sizes at different temperatures (or values of another coupling) are compared according to scaling laws for suitable observables with the goal of determining parameters of the system at the thermodynamic limit, such as the critical temperature or critical exponents. By exploiting the scaling forms, errors due to the fact that numerical values are only available for finite system sizes can be compensated, and it is often possible to make conclusions about the thermodynamic limit when only moderate system sizes are

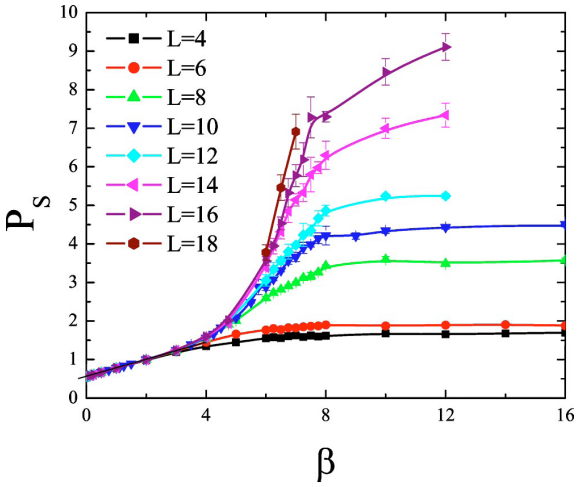

Figure 2.2: S-wave structure factor P_s as a function of inverse temperature β for the homogeneous AHM at various system sizes. The flattening of the curves at low temperature is indicative of a divergent correlation length and the onset of order. Reproduced from Ref. 45.

accessible. A key point in FSS is the divergence of correlation lengths at phase transitions.

Paiva et al. [45] provide an FSS for the superfluid transition of the homogeneous AHM. Some of the results are reproduced here to provide examples for the discussion of FSS in general, and context for the presentation of results from the confined system in Sec. 5.4.

Integrating a correlation function c which exhibits QLRO (2.9) over a two-dimensional system of linear size L yields the scaling behavior of the associated structure factor,

$$P \sim L^{2-\eta} f(L/\xi) =: L^{2-\eta} f(w), \tag{2.10a}$$

for large L, with a *scaling function* f and $w := L/\xi$. The correlation length scales as [42]

$$\xi \sim \exp \frac{A}{\sqrt{T - T_c}} \tag{2.10b}$$

with the critical temperature T_c and a parameter A. Note that the correlation length ξ diverges for all $T \leqslant T_c$, that is to say the system is critical in all of the KT phase.

On any finite system, the actual correlation length $\xi(T, L)$ is limited by the system size. Thus, as $T \to T_c^+$, the structure factor cannot grow to its

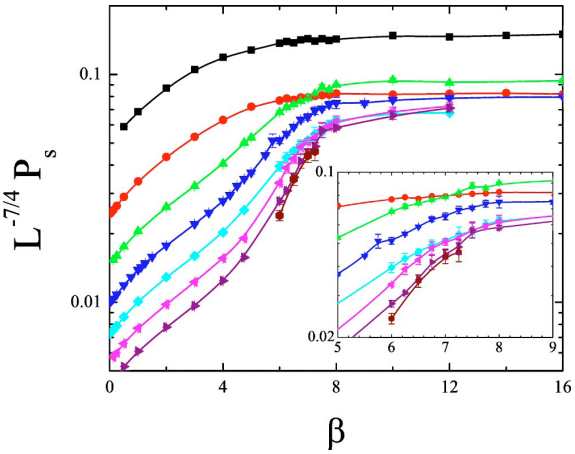

Figure 2.3: Scaled s-wave structure factor $L^{-7/4} P_s$ as a function of inverse temperature β for the homogeneous AHM at various system sizes. The convergence of the curves at low temperatures again indicates the divergence of the correlation length. The inset shows an enlargement of the region where the curves begin to coincide. Reproduced from Ref. 45.

thermodynamical value, but saturates when $\xi(T, L)$ ceases to increase. This behavior can be visualized by plotting $P(\beta, L)$ for various system sizes as a function of $\beta = 1/T$: At small β, where the system is disordered and ξ is small, the curves for all L will coincide. As β begins to grow, the finite system size is noticed and the curves begin to separate. Finally, as the transition is approached, the P saturate to the maximum values dictated by their respective L. An example of this kind of plot is shown in Fig. 2.2.

The same behavior may be visualized in a different way by bringing $L^{2-\eta}$ to the other side of (2.10a), and plotting $L^{\eta-2} P(\beta, L)$ as a function of β. In this case, the curves start out separated at low β but converge for large system sizes as the transition is approached. Fig. 2.3 shows an example.

If the scaling form of the correlation length (2.10b) is also taken into account, one arrives at a *scaling plot* as Fig. 2.4, where $f(w) = L^{\eta-2} P(\beta, w)$ is plotted (for $T > T_c$) as a function of w and one expects the curves for all system sizes to coincide. It is by looking for collapse on this plot that parameters are usually determined.

Lastly, in the critical region, because of the divergent correlation length, the unknown scaling function degrades to a proportionality constant,

$$P \sim f(0)\, L^{2-\eta} \qquad (T \leqslant T_c). \tag{2.11a}$$

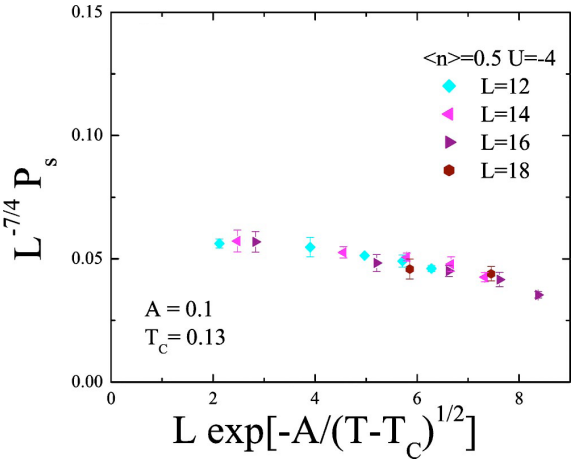

Figure 2.4: The scaling plot for the homogeneous AHM. The parameters T_c and A are varied to achieve a collapse of the curves for different system sizes L onto the scaling function f. The horizontal axis corresponds to $w = L/\xi$. Congruence of the curves implies that the scaling relations (2.10) hold and constitutes evidence for the KT transition. Reproduced from Ref. 45

Taking the logarithm, we see that

$$\log P \sim \big(2 - \eta(T)\big) \log L \qquad (T \leqslant T_c). \tag{2.11b}$$

At low temperature, the graphs of $\log P(T, L)$ as a function of $\log L$ become straight lines with the slope determined by η. In (2.11b), we have reinstated the explicit temperature dependence of η to emphasize that different slopes are expected for different temperatures.

3 Realizations of the Hubbard Model in Confined Systems

In recent years, experiments on ultra-cold atoms in optical lattices [17, 21, 28, 29, 36] have provided a novel realization of the Hubbard model. In contrast with solid-state systems, where the Hubbard Hamiltonian represents a highly abstracted model of the physical system, which one hopes may nonetheless capture the essence of the phenomena of interest, optical lattices are deliberately engineered to provide a realization of the Hubbard model or other lattice models. The hope is to gain insight into the model beyond what theoretical studies have been able to provide.

However, in the experiments it is necessary to confine the atoms to the region of the optical lattice. This confinement gives rise to an important modification of the Hamiltonian, in the form of an inhomogeneous potential unprecedented in condensed-matter systems.

In this chapter, after introducing the optical lattice Hamiltonian, the "local-density approximation" (LDA) for confined systems will be defined and the correct way to take the thermodynamic limit of confined systems will be presented. Finally, drawing heavily from the LDA, we will discuss some of the new physics of confined systems.

3.1 Optical Lattices

An *optical lattice* is essentially a standing light wave produced by intensive counterpropagating laser beams. Electrically neutral atoms interact with the electromagnetic field via the AC Stark effect. If the laser frequency ω is far detuned from an atomic transition, whose frequency we denote Ω, the standing light wave with position-dependent intensity $I(\vec{r})$ acts on the atoms as a periodic potential [36]

$$V(\vec{r}) \propto I(\vec{r})/\Delta \propto (\sin \vec{k} \cdot \vec{r})^2/\Delta$$

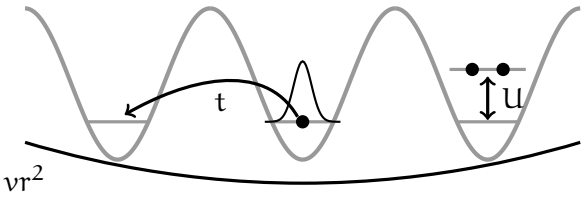

Figure 3.1: Schematic of an optical lattice with hopping matrix element t, interaction U and trapping potential νr^2. The horizontal direction represents position r, the vertical direction represents energy. The energy offset "$\updownarrow U$" represents an interaction between two atoms; only the lowest single-particle state in the potential well is involved.

where $\vec{k}$ is the wave vector of the laser beam and $\Delta := \omega - \Omega$ is the laser detuning. The sign of Δ determines which features of the standing wave attract the atoms: for a "red-detuned" beam, $\Delta < 0$, the antinodes become potential minima; in the "blue-detuned" case, $\Delta > 0$, the nodes are the minima.

If the potential is strong and the atoms have small kinetic energies, they become confined to the potential minima. In this way, a lattice model may be emulated, with the nodes or antinodes as analogues of the lattice sites and the atoms as particles. To emulate a single-band model, it is in fact required that the atoms occupy only the lowest-energy state in each of the potential wells.

Movement between the sites is possible by quantum tunneling; the tunneling amplitude t is given by an overlap integral over Wannier states at different sites, and depends quite sensitively on the depth of the lattice potential, i.e. on the intensity of the lasers. Since the tunneling rate decreases exponentially with the width of the barrier, it is typically assumed that only tunneling between nearest neighbors takes place, as in the tight-binding approximation in lattice models.

The interaction between atoms that share a "site" leads to an energy U associated with each pair of atoms on the site, which is proportional to the s-wave scattering length a_s [29]. The scattering length may be positive or negative and can be tuned in magnitude and sign via *Feshbach resonances* [12]. Because U also depends on the shape of the Wannier functions, it is affected by the depth of the lattice potential as well, but the dependence is much weaker than the hopping's.

Different types of atoms may be "loaded" into optical lattices; impor-

tantly, both "bosons" (e.g. ^{87}Rb) and "fermions" (e.g. ^{40}K, ^{6}Li) are available*. In the case of fermions, usually two different species (realized as different hyperfine states) are used to emulate the two spin states of electrons.

The number of particles in an optical lattice is fixed (disregarding losses, which have to be controlled in actual experiments). For calculations in the grand canonical ensemble, the chemical potential has to be adjusted so that the densities match. Magnetization may be emulated by introducing a population imbalance between atom species and is set by the magnetic field in the grand canonical description.

Systems of reduced dimensionality can be constructed by making the lattice potential so steep along one or two directions that an array of essentially decoupled one-dimensional tubes or two-dimensional sheets remains.

Thus, a realization of the attractive or repulsive, Fermi- or Bose-Hubbard model in one, two or three dimensions with highly tunable parameters can be constructed. In contrast to condensed-matter systems, the optical lattice is known to follow the model under relatively mild approximations. Time and length scales are much larger than in a solid, making e.g. the measurement of the particle density on a single site possible [4]. Lattice defects and phonons are absent. In these respects, optical lattices are a "purer" testing ground for the model than any other physical system.

However, an important modification to the Hubbard Hamiltonian (2.1) arises because of the *confining potential* which is needed in these experiments to confine the atoms to a region in space. Experimentally, this "*trap*" is typically realized as a magneto-optical trap. In the theoretical description, the trap may be modeled by a site-dependent chemical potential μ_i which is normally parabolic in the distance r_i (in units of the lattice spacing) from the trap center,

$$\mu_i = \mu_0 - \nu r_i^2 = \mu_0 - (r_i/\ell)^2\, t. \tag{3.1}$$

The trap introduces a length scale $\ell = \sqrt{t/\nu}$; the hopping t has been used as unit of energy. We note that the homogeneous case corresponds to the

*Of course, any atom is ultimately a compound of fermionic constituents, but for large enough separations, they interact as elementary fermions (odd number of constituents) or bosons (even number of constituents).

limit $\nu \to 0$ or $\ell \to \infty$. The full optical lattice Hamiltonian reads

$$\widehat{H} := -t \sum_{\langle ij \rangle\, \sigma} c^{+}_{\sigma i} c_{\sigma j} + U \sum_{i} (\widehat{n}_{\uparrow i} - 1/2)(\widehat{n}_{\downarrow i} - 1/2) - \sum_{i} (\mu_0 - \nu r_i^2)(\widehat{n}_{\uparrow i} + \widehat{n}_{\downarrow i}). \quad (3.2)$$

Here, we have not allowed for a magnetic field. In this work, we consider attractive ($U < 0$) fermions on a two-dimensional square lattice. Contrary to the model, the experiments have a fixed number of particles rather than a chemical potential, and evolve at constant entropy, since the system is essentially isolated [13, 30]. However, for large systems, the differences are expected to be negligible.

3.2 Local-Density Approximation

To study the effects of the trapping potential, instead of including it directly in a calculation, one may try to deduce the properties of the confined system from the corresponding homogeneous system. Each site i, with a local chemical potential μ_i, is identified with a homogeneous system $\widehat{H}_{\text{hom}} := \widehat{H}(t, U, \mu = \mu_i)$. In the context of confined systems, this idea is known as the *local-density approximation* (LDA)*.

At $t = 0$, where the system degenerates into a series of unconnected sites, the LDA becomes exact. Elsewhere, it is expected to hold whenever the density varies slowly as a function of position and the correlation length is not too large. Note that the first condition is not in general equivalent to a slowly varying chemical potential; the boundaries of a Mott-insulating region provide a counter-example (cf. Sec. 3.4).

The LDA has been widely used to study trapped systems, and for local observables, good agreement has generally been found where the above conditions are satisfied. Truly non-local quantities, such as correlations over large distances, cannot be calculated in the LDA since it does not

*Despite the name, this LDA is distinct from what is called the local-density approximation in density-functional theory.

In the present case, the name local-*density* approximation is actually an anticipation of the success of the LDA with regards to the particle density, since the primary definition used the chemical potential instead.

couple regions of different filling. For correlations over small distances, such as nearest-neighbor sites, the LDA can however give good results.

Part of the appeal of the LDA comes from the technical simplifications that follow. In DQMC, for example, the computational effort scales as the cube of the number of sites. Under the LDA, one has to carry out simulations of many homogeneous systems to compose one trapped system, but can typically use a much smaller system size* than with a true trap, such that the LDA calculation is less costly overall. This is what makes simulating very large fermionic systems possible, especially three-dimensional ones. For bosons, efficient algorithms exist that scale essentially linearly with the space-time volume, making direct simulations of large three-dimensional systems possible.

However, if one sees the ultimate goal of optical-lattice experiments in gaining information on *homogeneous* systems, e.g. determining the phase diagram of the homogeneous Hubbard model, the LDA appears in a different light: its validity becomes a prerequisite for success.

3.3 Thermodynamic Limit

In the presence of a confining potential, the usual thermodynamic limit† becomes ill-defined. It is not immediately clear whether an interesting thermodynamic limit including phase transitions can be recovered in the trap. Historically, these questions were first discussed‡ in the context of experiments on Bose-Einstein condensation (BEC) in harmonic traps, with no optical lattices involved at the time. It was found that a meaningful thermodynamic limit and phase transitions are possible. Indeed, in some cases a transition may appear in the trap that is absent in the homogeneous case; Mullin [43] discusses the example of noninteracting bosons in 2D, where a second-order phase transition to a BEC is forbidden by the Mermin-Wagner theorem [41] in the homogeneous case, but becomes possible in the trap because the density at the center diverges in the thermodynamic

*For example, the LDA results in this work were calculated on 8×8-systems, while 30×30 was the largest size of trapped systems simulated.

†Symbolically, $N \to \infty$, where N may stand for the number of particles, number of sites, or similar.

limit.

For a homogeneous system, one takes the thermodynamic limit at constant density, $\rho = \mathcal{N}/\mathcal{V} = \text{const}$ (number of particles $\mathcal{N}$, system volume $\mathcal{V}$). In effect, we imagine the system contained in a box and making that box bigger and bigger, while increasing the number of particles to keep the density constant. Using the grand canonical ensemble, one may simply keep the model parameters including the chemical potential constant and take $\mathcal{V} \to \infty$ to implement the limit.

For a trapped system, if the parameters including $\nu = t/\ell^2$ specifying the strength of the trap were kept constant, the system would not really scale at all; one would simply increase the empty area around an unchanged region of nonzero density, with the density averaged over the whole system approaching zero. In other words, the size of the system is really set by the trapping potential, which forces the density to zero outside some region; if we choose to imagine the system contained in a box, all that matters is that the box be big enough for that region.

In that sense, the linear size L of that box becomes irrelevant, and must be replaced with the trap length scale defined in (3.1); thus we arrive at the *characteristic density* in d dimensions $\widetilde{\rho} := \mathcal{N}/\ell^d = \mathcal{N}(\nu/t)^{d/2}$ or, for $d = 2$,

$$\widetilde{\rho} = \mathcal{N}/\ell^2 = \mathcal{N}\nu/t, \tag{3.3}$$

which must be kept constant in taking the thermodynamic limit*:

$$N \to \infty \qquad (\widetilde{\rho} = \text{const}). \tag{3.4}$$

It has been demonstrated numerically [47–49] that, using this prescription, different system sizes become comparable, and phase diagrams for trapped systems may be constructed.

For an additional point of view on the characteristic density, consider the following simple calculation, carried out for two dimensions. Using the LDA, and assuming a small lattice spacing or a continuous system, the number of particles in a trapped system may be calculated as an integral

‡See Ref. 43 and references therein.

*This prescription is implied in Ref. 43 but the characteristic density is not explicitly defined; rather, the requirement (3.4) is referred to as "constant average density".

over contributions determined by the local chemical potential

$$\begin{aligned}\mathcal{N} &= \int_0^R dr\, r\rho(r) = \tfrac{1}{2\nu}\int_{\mu_|}^{\mu_0} d\mu\, \rho(\mu) \\ &= \ell^2\, F(\mu_|, \mu_0)\end{aligned}$$

where $\rho(\mu) := \langle \widehat{n} \rangle_\mu$ is the density of the homogeneous system with chemical potential μ. In keeping with the argument above, we have used R, the radius beyond which the density becomes negligible, and the corresponding local chemical potential $\mu_| = \mu(R)$; as well as (3.1) in solving for $r(\mu)$ and $\nu = t/\ell^2$. Since $F(\mu_|, \mu_0)$ is determined by the model (μ_0 is a parameter and $\mu_|$ is a property of the model), it is clear that $\mathcal{N}/\ell^2$ must be constant.

From a practical point of view, if one wishes to simulate systems at various sizes for comparison or finite-size scaling, one may use the following procedure:

1. choose (linear) lattice sizes L_n to be simulated, usually as dictated by computing power
2. choose μ_0 to achieve a density at the trap center as required, ideally guided by results from the homogeneous model via the LDA
3. determine a local chemical potential $\mu_|$ at the edge of the simulated box such that the density will be negligible there, again guided by the LDA
4. compute a trap strength ν_n for each L_n such that $\mu(R_n) = \mu_0 - \nu_n R_n^2 = \mu_|$ where R_n is the minimum distance from the trap center to the edge of the box, usually $R_n = (L_n - 1)/2$.

This ensures that the characteristic density stays constant across the L_n. In fact, step 4 implies that the box size L (more precisely, $L - 1$) scales as the trap size ℓ, therefore the standard density will be constant as well as the characteristic density.

3.3.1 Trap-Size Scaling

In an FSS analysis for a confined system one must also take the trap into account, and use the length scale ℓ induced by the trap where the linear

system size L would be used in the homogeneous case. However, ℓ enters with a nontrivial new critical exponent, the *trap exponent* θ, which depends on the universality class of the model and the specific type of trap. The resulting modified FSS-scheme has been called *trap-size scaling* (TSS), see [10].

For the case of a classical KT-transition, Crecchi and Vicari [14] derive the trap exponent in the low-temperature limit and at the KT temperature T_c, finding $\theta = 1$ in both cases, and conjecture that this value holds for all of the QLRO regime,

$$\theta = 1 \qquad (T \leqslant T_c). \tag{3.5}$$

This would mean that the trap size ℓ enters as-is in the TSS; if one follows the recipe outlined above and keeps $L \propto \ell$, the same formulas may be used as in the standard FSS for a KT-transition [14, 44] as described in Sec. 2.5.

A further complication resulting from the trap concerns the critical exponent η, which determines the long-range behavior of the correlation function (2.9). In the homogeneous case, it is known that η is a function of temperature, increasing from $\eta = 0$ at $T = 0$ to $\eta = 1/4$ at T_c. As a universal property of the KT universality class, η can depend on the temperature only through the reduced temperature $T' := (T - T_c)/T_c$.

From an LDA point of view, one must consider T' and therefore $\eta = \eta(T')$ a local quantity, because T_c depends on the filling and therefore on position in the trap. In this sense, the long-range behavior of the correlation function, $c(r) \sim r^{-\eta} \exp(-r/\xi)$ in the homogeneous case (2.9), must be expected to change in the confined case. For the TSS scheme, the question arises whether an effective exponent η' exists such that the homogeneous-case scaling form of the structure factor, (2.10a) can be recovered as

$$P \sim \ell^{2-\eta'} f(\ell/\xi). \tag{3.6}$$

3.4 Coexistence of Phases

As we have seen in section Sec. 2.4, the phase of the Hubbard model depends on the chemical potential, and the local chemical potential depends on the position in the trap; therefore, the LDA predicts different phases to coexist at different locations in the trap. This effect was already pointed out by Jaksch et al. in the original proposal for an optical lattice filled

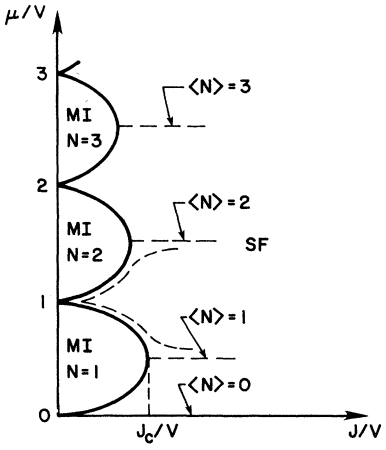

Figure 3.2: Schematic zero-temperature phase diagram of the homogeneous repulsive Bose-Hubbard model showing three Mott lobes, reproduced from Ref. 20. Here, the hopping is called J and the interaction V. In the LDA, traversing the trap from the center outward is tantamount to descending vertically in the diagram. Since the density has to decay to zero at the edges of a trapped system, the latter can never be in a pure MI state.

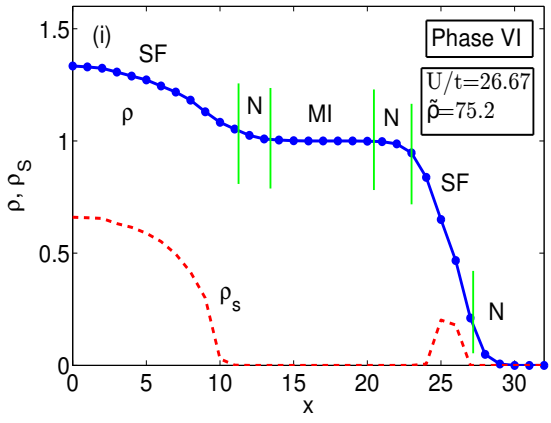

Figure 3.3: Coexistence of phases in the trapped 2D repulsive Bose-Hubbard model at $T = 1\,t$, reproduced from Ref. 40; x is the distance from the trap center, ρ the particle density and ρ_s the superfluid density. Superfluid (SF) regions are marked by a nonzero superfluid density, Mott insulator (MI) regions by a constant density. Note the region of normal (N) phase at the edge of the trap, which always exists at nonzero temperature.

with ultra-cold atoms [29], and has been confirmed in both numerical (see examples below) and experimental [21] studies. In a trapped system, the phases occur in a characteristic shell structure, with a disc of a high-density phase around the center followed by annuli of progressively lower density.

3.4.1 Repulsive Bosons

We begin with a discussion of the repulsive Bose-Hubbard model, where the phase coexistence is especially clear-cut, because lower temperatures (with respect to the energy scales of the model) can be reached, both

numerically and experimentally, and the phase diagram of the uniform model is well known.

The phase diagram of the bosonic RHM is customarily drawn in the $(t/U, \mu/U)$-plane; in the LDA, then, the trapped system traverses the homogeneous-case phase diagram at fixed t and spatially varying μ. At zero temperature, two kinds phases exist in the homogeneous system. At large hopping, the system is superfluid (SF). At small hopping, it enters a Mott-insulating phase (MI) which is characterized by an integer number of particles per site (*commensurate filling*). The critical t_c/U of the SF-MI transition is determined by μ; between MI-regions (often, "Mott lobes") with different filling, t_c/U is suppressed to zero. See Fisher et al. [20] for a discussion of the zero-temperature phase diagram, their schematic diagram is reproduced in Fig. 3.2. At nonzero temperature, a "normal" phase (N) intervenes between the MI and SF phases.

In a trapped system at nonzero temperature, SF and MI regions will alternate separated by N regions although only the N phase always appears. Mahmud et al. [40] show finite-temperature phase diagrams and discuss the combinations occuring in the trap, one example is reproduced in Fig. 3.3. MI regions are signaled by constant integer filling over a range of chemical potential and thus appear as flat steps ("Mott plateaux") in the density profile. This corresponds to the Mott gap or incompressibility (i.e. $d\rho/d\mu = 0$) in the homogeneous model, but note that the confined system is never globally incompressible or gapped, because the MI phase never occurs alone [5].

3.4.2 Repulsive Fermions

The situation is similar for fermions, except that low temperatures are more difficult to reach, and the phase diagram is not fully known, especially with regards to superfluidity.* Nevertheless, the MI phase has been reached and Mott plateaux are also seen. Here, the MI phase only exists at half-filling ($\rho = 1$); the completely filled ($\rho = 2$) state, which would appear as a similar plateau in the trap, is more properly called a band insulator as it does not

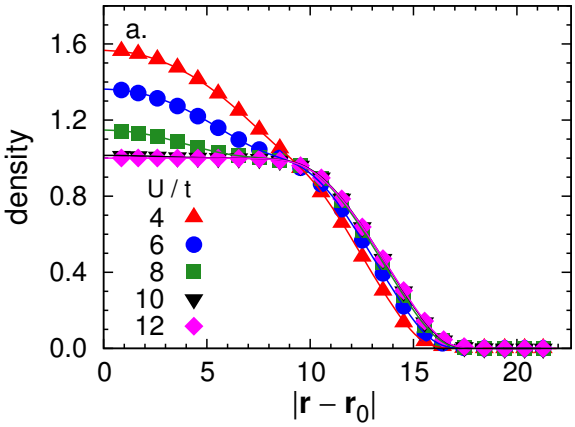

Figure 3.4: Coexistence of phases in the trapped 2D repulsive Fermi-Hubbard model, reproduced from Ref. 11. The density is shown for various values of the interaction at $T = 1/2\,t$ as a function of $|\mathbf{r} - \mathbf{r}_0|$, the distance from the trap center. At strong interactions, a Mott plateau is clearly seen to develop.

depend on the interaction.

3.4.3 Attractive Fermions

The reason why the MI phase and Mott plateau appear similarly for fermions and bosons is that it is a simple consequence of the repulsive interaction. If one imagines a homogeneous system with one particle on each site, there is an energy cost of order U to add a single additional particle to the system.

In the attractive case then, since that energy cost would be negative, it should come as no surprise that Mott plateaux do not occur. This may also be seen by means of the asymmetric particle-hole transformation (2.5): The Mott plateau at half-filling in the RHM is characterized by a vanishing compressibility $\kappa := d\rho/d\mu$. But the compressibility $\kappa(\mu)$ in the AHM is mapped to the magnetic susceptibility $\chi(h) := dm/dh$ in the RHM, which is known to be nonzero at $h = 0$. Therefore, the attractive case has no Mott plateau at half-filling.

For sufficiently low but nonzero temperatures, the LDA still predicts a coexistence of phases, namely, from the center outwards, SF, N, SF, N.

*In fact, understanding the phase diagram of of the fermionic RHM has been referred to as "the 'ultimate goal' of the theory of strongly correlated systems" [25]. Whether one wants to go that far or not, the question of d-wave superconductivity in the 2D RHM is certainly an important motivation for the continued interest in that model in general and the optical lattice experiments in particular.

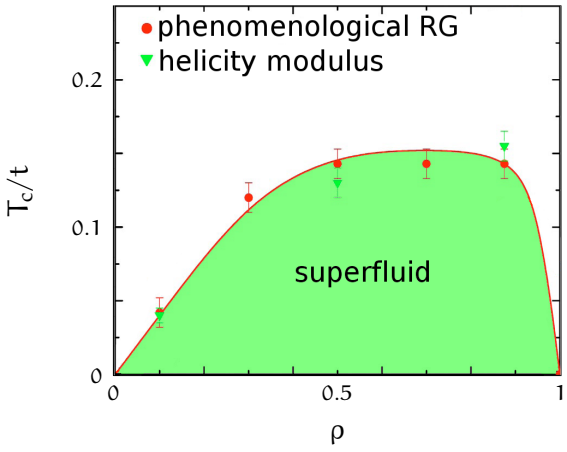

Figure 3.5: Phase diagram of the homogeneous 2D attractive Fermi-Hubbard model with $U = -4\,t$, adapted from Ref. 45. The KT transition temperature is shown as a function of the filling; the data are from quantum Monte Carlo simulations using two different methods to extract T_c. The line is only a guide to the eye. The phase diagram is symmetric about $\rho = 1$, with only one half shown. Note that T_c is suppressed to zero in a narrow region around half-filling.

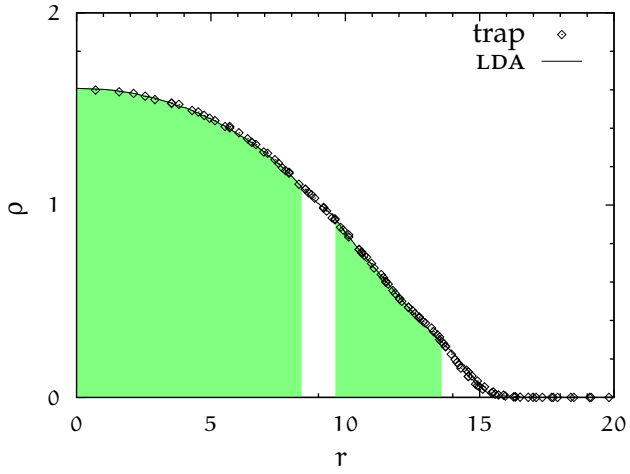

Figure 3.6: Coexistence of phases in the trapped 2D attractive Fermi-Hubbard model with $U = -6\,t$ at $T = 1/9\,t$. At low temperature, regions with a density which is not too close to an integer are expected to be superfluid (SF) under the LDA, cf. Fig. 3.5. For illustration, the expected SF regions are shown (shaded), using critical temperatures T_c from Fig. 3.5. Even though the interaction is stronger here, the regions are expected to be qualitatively correct since the dependence of T_c upon U is expected to weak. See Sec. 5.2 for a discussion of the validity of the LDA in this case.

However, this mixture is not visible from the density alone. See Figs. 3.5 and 3.6, and Sec. 5.2 for a detailed discussion.

4 Determinant Quantum Monte Carlo

Given a fermionic Hamiltonian $\hat{\mathcal{H}}$, we wish to evaluate thermodynamic expectation values

$$\langle \hat{A} \rangle = \frac{1}{Z} \operatorname{tr} \left\{ \hat{A} \, e^{-\beta \hat{\mathcal{H}}} \right\} = \sum_{|\psi\rangle} \langle \psi | e^{-\beta \hat{\mathcal{H}}} | \psi \rangle \tag{4.1}$$

with a hermitian operator $\hat{A}$, a complete basis $|\psi\rangle$, the inverse temperature $\beta := 1/T$ (using "$k_B = 1$"), and the partition function

$$Z = \operatorname{tr} \left\{ e^{-\beta \hat{\mathcal{H}}} \right\}. \tag{4.2}$$

In second quantized notation, $\hat{\mathcal{H}}$ is expressed as a function of the fermion creation and annihilation operators: $\hat{\mathcal{H}} = \mathcal{H}(\boldsymbol{c}^+, \boldsymbol{c})$. A particularly simple case is that of a *quadratic Hamiltonian*, where $\mathcal{H}$ is a quadratic form,

$$\hat{\mathcal{H}} = \sum_{i,j=1}^{M} c_i^+ h_{ij} c_j = \boldsymbol{c}^+ \boldsymbol{h} \, \boldsymbol{c}, \tag{4.3}$$

with a hermitian matrix $\boldsymbol{h}$. In this case, $\hat{\mathcal{H}}$ is encoded by the $M \times M$-matrix $\boldsymbol{h}$, where M is the number of single-particle states, whereas the matrix representing $\hat{\mathcal{H}}$ in Fock space is of the size $2^M \times 2^M$. Note that being quadratic is a basis-independent property of an operator; a change of basis can merely change the elements of $\boldsymbol{h}$.

As a simple example of how calculations are simplified when the Hamiltonian is quadratic, consider the partition function (4.2). If (4.3) holds, we have

$$Z = \operatorname{tr}_{2^M} \left(e^{-\beta \hat{\mathcal{H}}} \right) \overset{(4.3)}{=} \det{}_M \left(\boldsymbol{I}_M + e^{\boldsymbol{h}} \right), \tag{4.4}$$

which is easily seen in the eigenbasis of $\boldsymbol{h}$.

More physically put, a Hamiltonian of the form (4.3) has only hopping terms with coefficients $h_{i\neq j}$ and potential terms with coefficients h_{ii}. Thus, it describes a system of non-interacting particles.

In *Determinant Quantum Monte Carlo* (DQMC), one maps an interacting system, where $\mathcal{H}(\mathbf{c}^+, \mathbf{c})$ contains quartic terms, to a series of non-interacting systems of the form (4.3); then, traces such as (4.1) relative to these systems may be carried out explicitly.

In the following sections, we will sketch the DQMC scheme for the Hubbard model (2.1) as developed by Blankenbecler, Sugar, and Scalapino [8] with local interactions U, nearest-neighbor hopping t and a spatially varying potential μ_i. Spatially varying interactions U_i or arbitrary hoppings t_{ij} represent a trivial generalization, but will not be used here.

What is attempted here is a presentation of the ideas in DQMC, not a complete description of a practical DQMC program. For more detailed reviews, see for example [39, 55].

4.1 Hubbard-Stratonovich Transformation

The mapping from an interacting Hamiltonian, such as the Hubbard model $\widehat{H}$ (2.1), to non-interacting Hamiltonians of the form (4.3) is accomplished by the *Hubbard-Stratonovich transformation* (HST). One introduces auxiliary variables ("HS fields"), which have subsequently to be integrated out in order to restore the original, physical, quantities. Different mappings of this sort are possible. The auxiliary variables may be interpreted as massless bosonic fields that couple to the fermions, which now are non-interacting.

In the original HST, these fields take on a continuous range of values [26, 53]. In the version described here (discrete HST), which has proven more practical for simulations [22, 55], the fields may only take the values ± 1. As described here, the procedure is specifically geared towards an on-site density-density interaction as it appears in the Hubbard model (2.1), but other cases are possible, for example extended interactions [39, App. I].

The aim is to recast the exponential of the interaction term $(\widehat{n}_\uparrow - 1/2)(\widehat{n}_\downarrow - 1/2) = (c^+_\uparrow c_\uparrow - 1/2)(c^+_\downarrow c_\downarrow - 1/2)$, which is quartic in fermion operators, in a quadratic form. First, we write it in terms of a complete

square, as one of

$$(\hat{n}_\uparrow - 1/2)(\hat{n}_\downarrow - 1/2) = \frac{1}{2}\Big[(\hat{n}_\uparrow + \hat{n}_\downarrow - 1)^2 - 1/2\Big] \tag{4.5a}$$

or

$$(\hat{n}_\uparrow - 1/2)(\hat{n}_\downarrow - 1/2) = -\frac{1}{2}\Big[(\hat{n}_\uparrow - \hat{n}_\downarrow)^2 - 1/2\Big]. \tag{4.5b}$$

In each case, the operator $\hat{X}$ under the square has the properties

$$\hat{X}^{2\nu} = \hat{X}^2, \tag{4.6a}$$

$$\hat{X}^{2\nu+1} = \hat{X} \tag{4.6b}$$

for all positive integers ν, which is easily verified using the identity $\hat{n}_\sigma^2 = \hat{n}_\sigma$. Using this, we conclude

$$\begin{aligned} e^{\gamma\hat{X}^2} &= 1 + \sum_{\nu=1}^{\infty} \frac{\gamma^\nu}{\nu!}\hat{X}^2 \\ &= 1 + \hat{X}^2(e^\gamma - 1); \\ e^{\lambda\hat{X}} &= 1 + \sum_{\nu=1}^{\infty}\left\{\frac{\lambda^{2\nu-1}}{(2\nu-1)!}\hat{X} + \frac{\lambda^{2\nu}}{(2\nu)!}\hat{X}^2\right\} \\ &= 1 + \sinh(\lambda)\,\hat{X} + (\cosh\lambda - 1)\,\hat{X}^2, \end{aligned}$$

therefore,

$$\tfrac{1}{2}\big(e^{\lambda\hat{X}} + e^{-\lambda\hat{X}}\big) = 1 + \hat{X}^2(\cosh\lambda - 1),$$

which allows us to write

$$e^{\gamma\hat{X}^2} \overset{(4.6)}{=} \frac{1}{2}\sum_{s=\pm 1} e^{s\lambda\hat{X}} \tag{4.7a}$$

provided

$$\cosh\lambda = \exp\gamma. \tag{4.7b}$$

This is already the basic HST in the form it will be used in this work. Note that for positive γ the parameter λ is real, while for negative γ it is imaginary; for a negative γ, we may alternatively use the real $\lambda' := i\lambda$ and write $\cos\lambda' = \exp\gamma < 1$.

4.2 Suzuki-Trotter Decomposition

The identities (4.7) and (4.5) show how an operator $e^{-\beta U(\hat{n}_\uparrow - 1/2)(\hat{n}_\downarrow - 1/2)}$ can be recast in the desired form, but we are not yet in a position to apply this idea because, in addition to the interaction part $\widehat{U}$ that we wish to rewrite, $\widehat{H} = \widehat{K} + \widehat{U}$ (or any non-trivial Hamiltonian) also contains a kinetic part $\widehat{K}$, which fails to commute with $\widehat{U}$. Here, $\widehat{K}$ is intended to contain all terms of the Hamiltonian that are already quadratic, i.e. also a chemical potential or magnetic field in addition to the hopping, so that $\widehat{U}$ is left with only the on-site interaction.

Therefore, we employ the *Suzuki-Trotter decomposition* [54] to separate the two parts:

$$\begin{aligned} e^{-\beta \widehat{H}} &= \left[e^{-\beta/M(\widehat{K}+\widehat{U})}\right]^M = \prod_{\tau=1}^{M} e^{-\Delta\tau(\widehat{K}+\widehat{U})} \\ &\simeq \prod_{\tau=1}^{M} e^{-\Delta\tau \widehat{K}}\, e^{-\Delta\tau \widehat{U}} \\ &= \prod_{\tau=1}^{M} \left\{ e^{-\Delta\tau \widehat{K}} \prod_{i=1}^{N} e^{-\Delta\tau U(\hat{n}_{\uparrow i} - 1/2)(\hat{n}_{\downarrow i} - 1/2)} \right\} \end{aligned} \tag{4.8}$$

where $\Delta\tau = \beta/M$, the second product runs over all lattice sites and we have neglected terms of order $\Delta\tau^2 tU$ in the second line.

4.3 Application to the Hubbard Model

The HST for one piece of the Suzuki-Trotter decomposition (4.8), using (4.5) and (4.7), reads either

$$\exp\{-\Delta\tau U(\hat{n}_{\uparrow i} - 1/2)(\hat{n}_{\downarrow i} - 1/2)\} = e^{\Delta\tau U/4} \frac{1}{2} \sum_{s=\pm 1} \exp\{\lambda s \left[\hat{n}_{\uparrow i} + \hat{n}_{\downarrow i} - 1\right]\} \tag{4.9a}$$

with

$$\cosh\lambda := e^{-\Delta\tau U/2}; \tag{4.9b}$$

or

$$\exp\{-\Delta\tau U(\hat{n}_{\uparrow i} - 1/2)(\hat{n}_{\downarrow i} - 1/2)\} = e^{-\Delta\tau U/4} \frac{1}{2} \sum_{s=\pm 1} \exp\{\lambda s \left[\hat{n}_{\uparrow i} - \hat{n}_{\downarrow i}\right]\} \quad (4.10a)$$

this time with

$$\cosh\lambda := e^{+\Delta\tau U/2}. \quad (4.10b)$$

As noted before, λ for a given variant of the transformation will be real or imaginary depending on sign of U; and for a given $U \neq 0$, exactly one variant will give a real λ. In principle, the choice between the two variants (or any other form of HST) is completely arbitrary, but for numerical simulations, one usually chooses a real λ, and therefore (4.9) for $U < 0$ and (4.10) for $U > 0$, in order to avoid the additional effort of working with complex variables. It is in this sense that the conditional equation for λ is sometimes written $\cosh\lambda = e^{\Delta\tau|U|/2}$.

For future reference, we note another difference between the two transformations: In the first, the field s couples to the charge of the fermions, whereas in the second, it couples to the spin. Thus the variant (4.9) has been termed "SU(2)-symmetric" [2], since the SU(2) spin symmetry of the original model is preserved for every configuration of the HS fields individually, whereas in the case of (4.10), which arbitrarily singles out the z-component of the spin, spin symmetry is only restored upon summation over all field configurations.

In the negative-U case, Assaad [2] has shown that using the SU(2)-symmetric decomposition (4.9) can greatly improve the fluctuations of the estimators for spin correlations in the xy-plane, at the expense of using complex numbers in the calculations.

This difference between the two HST variants will also be relevant for the discussion of the numerical sign problem of DQMC in Sec. 4.4.3.

4.4 DQMC Scheme for the Hubbard Model

Combining the Suzuki-Trotter decomposition with the HST, we have

$$\begin{aligned} e^{-\beta \widehat{H}} &\overset{(4.8)}{\simeq} \prod_{\tau} e^{-\Delta\tau \widehat{K}} \prod_{i} e^{\Delta\tau U/4} \sum_{s(i,\tau)} e^{\lambda s(i,\tau) \left[\widehat{n}_{\uparrow i} + \widehat{n}_{\downarrow i} - 1\right]} \\ &\overset{(4.9)}{=} \left[\frac{e^{\Delta\tau U/4}}{2}\right]^{NL} \sum_{\{s\}} \prod_{\tau} e^{-\Delta\tau \widehat{K}} \prod_{i} e^{\lambda s(i,\tau) \left[\widehat{n}_{\uparrow i} + \widehat{n}_{\downarrow i} - 1\right]} \\ &=: \left[\frac{e^{\Delta\tau U/4}}{2}\right]^{NL} \sum_{\{s\}} \prod_{\tau} e^{-\Delta\tau \widehat{K}} e^{-\Delta\tau \widehat{U}_{\tau}} \end{aligned} \tag{4.11}$$

where $\sum_{\{s\}}$ runs over all configurations of the fields $s(i,\tau)$ and $\widehat{U}_{\tau}$, which represents the interaction after the HST, depends on the time slice via the HS fields. We chose the SU(2)-symmetric HST (4.9) because it is the usual one for the attractive Hubbard model and was used in the numerical part of this work.

Instead of the original interacting problem, we are thus left with a sum over non-interacting problems; it is this sum that will be carried out by Monte Carlo.

By the linearity of the trace, the sum over configurations $\{s\}$ is inherited by the partition function, $Z = \sum_{\{s\}} Z(\{s\})$. Furthermore, because the two spin species are completely independent within each term of the sum, the partition function may be factorized as $Z(\{s\}) = Z_{\uparrow}(\{s\}) Z_{\downarrow}(\{s\}) = \mathrm{tr}(e^{-\Delta\tau \widehat{H}_{\uparrow}}) \,\mathrm{tr}(e^{-\Delta\tau \widehat{H}_{\downarrow}})$ where $e^{-\Delta\tau \widehat{H}_{\sigma}}$ stands for all the factors acting on spin σ which appear in the term with fields $\{s\}$.*

To further rewrite the partition function, we need a generalization of (4.4) appropriate for a Suzuki-Trotter product of bilinear operators. Indeed, it can be shown [39] that

$$\mathrm{tr}\left\{e^{-\Delta\tau \widehat{\mathcal{H}}_1} \cdots e^{-\Delta\tau \widehat{\mathcal{H}}_M}\right\} = \det\left\{\boldsymbol{I} + e^{-\Delta\tau \boldsymbol{h}_1} \cdots e^{-\Delta\tau \boldsymbol{h}_M}\right\} \tag{4.12}$$

*More formally, each contribution to the partition function may be written as $\mathrm{tr}(\widehat{O}_{\uparrow}\widehat{O}_{\downarrow})$ where $\widehat{O}_{\sigma}$ only acts on the σ-subspace of the Fock space. Writing every Fock state as a tensor product of states from the spin subspaces, $|\psi\rangle = |\psi_{\uparrow}\rangle \otimes |\psi_{\downarrow}\rangle$, we have $Z(\{s\}) = \sum_{\psi_{\uparrow},\psi_{\downarrow}} \langle\psi_{\uparrow}|\widehat{O}_{\uparrow}|\psi_{\uparrow}\rangle \langle\psi_{\downarrow}|\widehat{O}_{\downarrow}|\psi_{\downarrow}\rangle = \mathrm{tr}_{\uparrow}\, \widehat{O}_{\uparrow}\ \mathrm{tr}_{\downarrow}\, \widehat{O}_{\downarrow}$.

if $\hat{\mathcal{H}}_n =: \boldsymbol{c}^+ \boldsymbol{h}_n \boldsymbol{c}$, which yields the expression

$$Z = \sum_{\{s\}} \det \boldsymbol{M}_\uparrow \, \det \boldsymbol{M}_\downarrow \tag{4.13a}$$

for the partition function, where

$$\boldsymbol{M}_\sigma := \boldsymbol{I} + \boldsymbol{B}_1^\sigma \cdots \boldsymbol{B}_M^\sigma \tag{4.13b}$$

and

$$\boldsymbol{B}_\tau^\sigma := e^{-\Delta\tau \boldsymbol{k}} \, e^{-\Delta\tau \boldsymbol{u}_\tau^\sigma} \tag{4.13c}$$

with $\boldsymbol{k}$ and $\boldsymbol{u}_\tau^\sigma$, the matrices representing the bilinear operators $\hat{K}^\sigma$ and $\sum_i \lambda s(i,\tau)\hat{n}_{\sigma i}$, respectively. We do not write a spin index on $\boldsymbol{k}$ because it is identical for both spins.* Note that $\boldsymbol{M}$, $\boldsymbol{B}$ and $\boldsymbol{u}$ implicitly depend on $\{s\}$.

For a Monte Carlo simulation, (4.13) means that the weight of a configuration $\{s\}$ is given by

$$Z(\{s\}) := \det \boldsymbol{M}_\uparrow \det \boldsymbol{M}_\downarrow. \tag{4.14}$$

Because the trace which is encoded in (4.13) sums over all occupation numbers $n(i,\tau)$, DQMC automatically works in the grand canonical ensemble. The particle density is set by the chemical potential μ.

4.4.1 Green's Functions and Measurements

In the formalism of DQMC leading up to (4.11), any thermodynamic expectation value takes a similar form as the partition function,

$$\begin{aligned}\langle \hat{A} \rangle &= \tfrac{1}{Z} \operatorname{tr}\left(\hat{A} \, e^{-\beta \hat{H}} \right) \simeq \tfrac{1}{Z} \sum_{\{s\}} \operatorname{tr}\left(\hat{A} \prod_\tau e^{-\Delta\tau \hat{K}} e^{-\Delta\tau \hat{U}_\tau} \right) \\ &=: \tfrac{1}{Z} \sum_{\{s\}} A(\{s\}) = \tfrac{1}{Z} \sum_{\{s\}} Z(\{s\}) \langle A \rangle_{\{s\}}.\end{aligned}$$

where $\langle \cdot \rangle_{\{s\}} = 1/Z(\{s\}) \operatorname{tr}(\cdot)$ denotes a thermodynamic expectation value with respect to the effective Hamiltonian of the configuration $\{s\}$.

*So is $\boldsymbol{u}$ for the SU(2)-symmetric HST.

For each configuration of fields, since one effectively solves a quadratic Hamiltonian, Wick's theorem applies, and all observables may be written in terms of the *single-particle Green's functions* [39, 55]

$$G^{\sigma}_{ij}(\{s\}) := \langle c_{\sigma i}\, c^{+}_{\sigma j}\rangle_{\{s\}}. \tag{4.15}$$

Symbolically, $\langle A\rangle_{\{s\}} = \mathcal{A}\big(G^{\sigma}_{ij}(\{s\})\big)$ with the precise form of $\mathcal{A}$ determined by the form of $\widehat{A}$ in terms of creation and annihilation operators. This does not imply that Wick's theorem holds for the complete model; the property is lost in the sum over the HS fields.

If we have access to the Green's functions for every configuration, it is thus easy to derive observables from a stream of field configurations given by a Monte Carlo simulation.

As an example, for the s-wave correlation function (2.2b) we have

$$\begin{aligned} c_{\text{pair}}(i, j; \{s\}) &= \langle \Delta^{+}_{i}\Delta_{j} + \Delta^{+}_{j}\Delta_{i}\rangle_{\{s\}} \\ &= \langle c^{+}_{\uparrow i}c^{+}_{\downarrow j}c_{\uparrow j}c_{\downarrow i} + c^{+}_{\uparrow j}c^{+}_{\downarrow j}c_{\downarrow i}c_{\downarrow j}\rangle_{\{s\}} \\ &= \langle c^{+}_{\uparrow i}c_{\uparrow j}\rangle_{\{s\}}\langle c^{+}_{\downarrow i}c_{\downarrow j}\rangle_{\{s\}} + \langle c^{+}_{\uparrow j}c_{\uparrow i}\rangle_{\{s\}}\langle c^{+}_{\downarrow j}c_{\downarrow i}\rangle_{\{s\}} \\ &= (\delta_{ij} - G^{\uparrow}_{ji})(\delta_{ij} - G^{\downarrow}_{ji}) + (\delta_{ji} - G^{\uparrow}_{ij})(\delta_{ji} - G^{\downarrow}_{ij}) \end{aligned} \tag{4.16}$$

because contractions of operators with opposite spins vanish, $\langle c^{+}_{\uparrow}c_{\downarrow}\rangle_{\{s\}} = 0$, since the spin species are decoupled; this is also why we were able to write the Green's functions separately for each spin species. In the last line of the equation, the dependence on $\{s\}$ is suppressed for brevity, and the Kronecker symbols δ_{ij} are necessary to restore the operator order demanded by the definition (4.15).

Computation of the $G^{\sigma}_{ij}(\{s\})$ from $\{s\}$ is facilitated by a formula analogous to (4.12), which may be derived by introducing a field J coupling to $c_{\sigma i}c^{+}_{\sigma j}$ in the action, and taking a derivative at $J = 0$, see [39, Sec. 3.4]. Writing the spin-σ Green's functions as a matrix $\boldsymbol{G}^{\sigma}$ and dropping the explicit dependence on the fields for simplicity, the result reads

$$\boldsymbol{G}^{\sigma} = \boldsymbol{M}_{\sigma}^{-1} = \left[\boldsymbol{I} + \boldsymbol{B}^{\sigma}_{M}\cdots\boldsymbol{B}^{\sigma}_{2}\boldsymbol{B}^{\sigma}_{1}\right]^{-1}. \tag{4.17}$$

In a numerical calculation, care must be taken in the matrix multiplications and inversion when using this formula. At low temperatures and strong

interactions, the elements of the $\boldsymbol{B}$ matrices can span many orders of magnitude and the product becomes more and more ill-conditioned. To ensure correct results, numerical stabilization techniques, e.g. involving SVD decomposition of the matrices, must be used [3].

Although formally all imaginary times are equivalent, in the course of a simulation we will also have occasion to use the Green's function at some imaginary time τ; this is given by [39]

$$\boldsymbol{G}^{\sigma}(\tau,\tau) = \left[\boldsymbol{I} + \boldsymbol{B}^{\sigma}_{\tau-1}\boldsymbol{B}^{\sigma}_{\tau-2}\cdots\boldsymbol{B}^{\sigma}_{1}\,\boldsymbol{B}^{\sigma}_{M}\cdots\boldsymbol{B}^{\sigma}_{\tau}\right]^{-1}.$$

Note that the Green's function matrix at any imaginary time may be used to compute the weight $Z(\{s\})$ (which depends on the HS fields at all imaginary times). By Sylvester's determinant theorem, $\det(\boldsymbol{I}+\boldsymbol{AB}) = \det(\boldsymbol{I}+\boldsymbol{BA})$, and thus

$$\begin{aligned}\det\left(\boldsymbol{G}^{\sigma}(\tau,\tau)\right)^{-1} &= \det\left[\boldsymbol{I} + (\boldsymbol{B}^{\sigma}_{\tau-1}\cdots\boldsymbol{B}^{\sigma}_{1})\,(\boldsymbol{B}^{\sigma}_{M}\cdots\boldsymbol{B}^{\sigma}_{\tau})\right]\\ &= \det\left[\boldsymbol{I} + (\boldsymbol{B}^{\sigma}_{M}\cdots\boldsymbol{B}^{\sigma}_{\tau})\,(\boldsymbol{B}^{\sigma}_{\tau-1}\cdots\boldsymbol{B}^{\sigma}_{1})\right]\\ &= \det\boldsymbol{M}_{\sigma}.\end{aligned}$$

Finally, though we have limited ourselves to static observables here, it is possible to calculate unequal-time Green's functions $\boldsymbol{G}^{\sigma}(\tau,\tau')$ and dynamical observables.

4.4.2 Local Updates

Recomputing the matrices $\boldsymbol{M}_{\sigma}$, their determinants and their inverses from scratch for each $\{s\}$ would be prohibitively expensive for simulations of large systems. If one limits oneself to local updates of the form $s(i,\tau) \leftarrow -s(i,\tau)$ ("flipping" a single HS field at a time, which also helps to keep the probability to accept proposed moves large enough), it is possible to derive simple formulas for updating the Green's functions and calculating the ratio of determinants which enters the acceptance probability for the flip. For the SU(2)-symmetric HST, it can be shown [39, Sec. 3.5, with a straightforward modification to account for the different HST used] that

$$\frac{\det\boldsymbol{M}'_{\sigma}}{\det\boldsymbol{M}_{\sigma}} \overset{(4.9)}{=} e^{\lambda[s'(i,\tau)-s(i,\tau)]}\left(1 + G^{\sigma}_{ii}(\tau)\right).$$

Note that only the current field configuration and Green's functions enter; the matrices $\boldsymbol{M}_\sigma$ themselves have become dispensable, and the Green's functions $\boldsymbol{G}^\sigma$ are now the central objects of the simulation.

4.4.3 Sign Problem

In the weight (4.14), each determinant can be positive or negative (when λ is real), or have an arbitrary complex phase (when λ is imaginary). Therefore, one must expect a sign or phase associated with the weight $Z(\{s\})$; in other words, DQMC suffers from the numerical sign problem [6, 38]. Whether a sign problem actually exists depends on the type of interaction, attractive or negative, encoded by $\operatorname{sgn}(U)$, as well as the type of HST. We will examine each of the four cases, $U > 0$ or $U < 0$ and (4.9) or (4.10), separately.

$U < 0$, λ real
The fields couple to $\hat{n}_\uparrow + \hat{n}_\downarrow$ (4.9). All quantities are real and equal for both spins, in particular $\det \boldsymbol{M}_\uparrow = \det \boldsymbol{M}_\downarrow$ and hence $Z(\{s\}) = (\det \boldsymbol{M}_\sigma)^2 > 0$, there is no sign problem.

$U < 0$, λ imaginary
The fields couple to $\hat{n}_\uparrow - \hat{n}_\downarrow$ (4.10). Since λ is purely imaginary, $\boldsymbol{M}_\downarrow = \boldsymbol{M}_\uparrow^*$, hence $Z(\{s\}) = |\det \boldsymbol{M}_\sigma|^2 > 0$, there is no sign problem.

$U > 0$, λ real
The fields couple to $\hat{n}_\uparrow - \hat{n}_\downarrow$ (4.10). Since λ is real and the coupling is different for the two spin species, $\operatorname{sgn}(\det \boldsymbol{M}_\uparrow)$ is in general independent from $\operatorname{sgn}(\det \boldsymbol{M}_\downarrow)$, and a sign problem exists.

$U > 0$, λ imaginary
The fields couple to $\hat{n}_\uparrow + \hat{n}_\downarrow$ (4.9). Again $\boldsymbol{M}_\uparrow = \boldsymbol{M}_\downarrow$ holds, but since the matrices are complex, this does not restrict the phase of $Z(\{s\})$, so that a phase problem exists.

We see that DQMC is protected from the sign problem in the case of the attractive ($U < 0$) Hubbard model, whereas it is subject to a sign or phase problem for the repulsive ($U > 0$) model. It should be noted that these statements are specific to the transformations (4.9) and (4.10).

In the above, we silently assumed that there is no external magnetic field ($h = 0$), which would destroy the protection from the sign problem of the attractive model. A more complete statement is thus, there is no sign problem for

- the attractive model at $h = 0$ and any μ, and
- the repulsive model at half-filling ($\mu = 0$) and any h [23].

In the context of the Hubbard model, one is usually more interested in a doped system (i.e., $\mu \neq 0$) than in a magnetic field; also, in the presence of a trapping potential, $\mu = 0$ is never globally true.* In this sense, the sign problem affects the repulsive model and not the attractive one.

Note that the two cases above are connected by the asymmetric particle-hole transformation (Sec. 2.3.2); similarly, it connects the cases with sign problem with each other. In other words, one cannot use a particle-hole transformation to circumvent the sign problem.

Finally, non-interacting fermions ($U = 0$), are a special case, which DQMC solves exactly. This is because the Suzuki-Trotter decomposition (4.8) becomes exact for any M and every $\{s\}$ gives the same contribution, since the fermions decouple from the fields.

4.5 DQMC Codes Used in this Work

The main calculations for this work were carried out using the DQMC package QUEST [35]. The DQMC framework as well as code to simulate trapped systems were already provided; for this work, QUEST merely had to be modified to support $U < 0$ and the measurement of c_{pair} (2.2b).

Some additional calculations were carried out using a DQMC program developed by Dahnken [15], see Sec. 5.3.

The results in this work were obtained from tens of thousands of sweeps distributed over several independent simulations, after an equilibration of typically 1000 sweeps each. Autocorrelations were found to be small for the observables measured. An imaginary-time step of $\Delta\tau = 0.1/t$ was used in the calculations for the finite-size extrapolation, and $\Delta\tau = 0.125/t$ for all other calculations.

*In the recently proposed off-diagonal confinement scheme [50], which we briefly describe in Sec. 5.2, $\mu = 0$ can be true for the whole system.

5 Results

In this chapter, we present DQMC results for a trapped system at $\beta = 9/t$ with $U = -6\,t$, $\mu = 0.8\,t$, and $v = 0.0097\,t$, thus $\ell \simeq 10$. We compare results from the LDA (obtained on 8×8-lattices) with a true confined system, which was simulated on a 30×30-lattice. The characteristic density for this system is $\widetilde{\rho} = 5.47(2)$.

Next, we present a finite-size extrapolation from trapped systems of lattice sizes $L = 12, 14, \ldots, 24$ at inverse temperatures between $\beta = 1 \ldots 16$. Here, the characteristic density varies with the temperature, between $\widetilde{\rho} \simeq 6.3$ at high temperature and $\widetilde{\rho} \simeq 5.1$ at low temperature.

5.1 Density Profile and the LDA

Fig. 5.1 shows results for the particle density of homogeneous systems at sizes 6×6 and 8×8 as a function of chemical potential μ, and illustrates how the LDA is constructed by mapping the μ to the radius r in the trap, using the inverse of (3.1),

$$r(\mu) = \sqrt{\frac{\mu_0 - \mu}{v}}.$$

No difference is seen between the two sizes, which indicates that finite-size errors for local quantities are already small for these system sizes.

The LDA results from 8×8 are shown again in Fig. 5.2 and compared to the density profile of the trapped 30×30-system. In this case, the LDA performs perfectly. This data was already shown in Fig. 3.6.

In contrast to the RHM, there is no Mott gap in the homogeneous case and correspondingly no plateau at half-filling in the trapped system,* cf. Fig. 3.4 and the discussion in Sec. 3.4.3.

*This is in contrast to results from dynamical mean field theory recently reported by Koga et al. [31], who find a supersolid region with $\rho = 1$ and CDW order around half-filling.

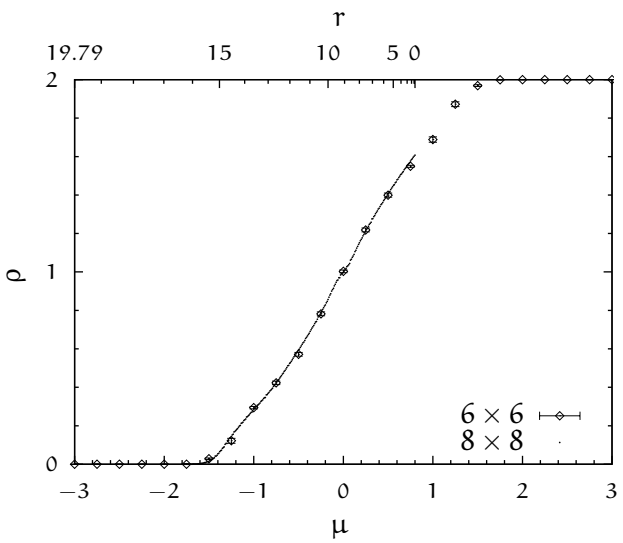

Figure 5.1: Density $\rho(\mu)$ of the homogeneous AHM as a function of chemical potential. The axis on top shows how μ is mapped to radius r in the 30×30-system within the LDA (no results from the trapped system are shown in this plot). The large circles with error bars show results calculated on a 6×6-lattice, the small dots show the high-resolution results used for Figs. 5.2 and 3.6 (the uncertainties are smaller than for the 6×6-results). The density is symmetric about $\mu = 0$ as required by particle-hole symmetry. It is also seen that finite-size errors for local quantities are small already at these sizes.

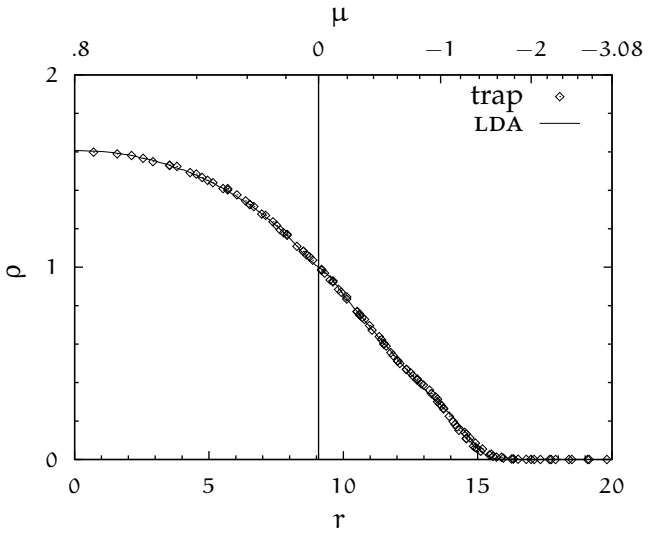

Figure 5.2: Density profile $\rho(r)$ of the 30×30-system. One point is shown for every lattice site of the confined system (up to lattice symmetry) and the LDA-results from Fig. 5.1 are shown as a solid line, the half-filled point is indicated by a vertical line. Perfect agreement is found for the density. The error bars for the trapped system are smaller than the symbols.

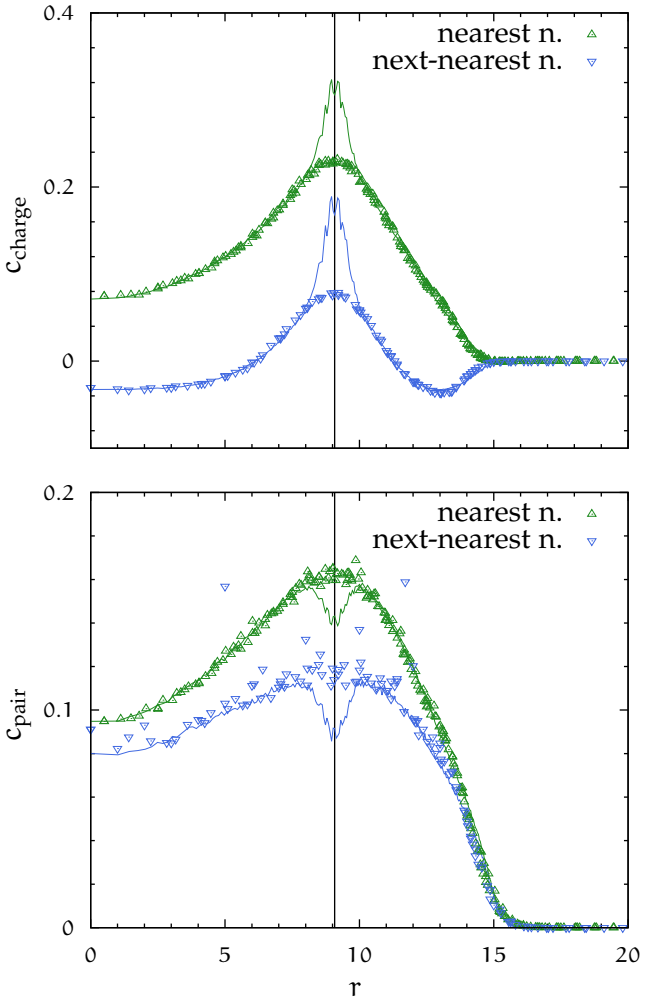

Figure 5.3: CDW and s-wave pairing correlations of the 30×30-system in the LDA (solid line) and the confined system. While good agreement is found elsewhere, at half-filling (marked by a vertical line) the LDA clearly fails (see text). We show nearest-neighbor and next-nearest-neighbor correlations, which the LDA is able to describe although they are not truly local. In the case of next-nearest neighbors, the sign of c_{charge} is reversed. Error bars are not shown to avoid clutter; for c_{charge} they are typically smaller than the symbols, for c_{pair} the fluctuations described in Sec. 5.3 result in larger uncertainties.

5.2 Correlations and Failure of the LDA

Fig. 5.3 shows the correlation functions c_{charge} and c_{pair} for the 30×30-lattice. In both cases, the LDA predicts a sharp feature (peak or dip) near half-filling; in both cases that feature is absent in the true confined system. Thus, we observe a drastic failure of the LDA in a case where it is expected to hold, according to the criterion of smoothly varying density outlined in Sec. 3.2.

The LDA result may be understood in the context of the homogeneous-case phase diagram in Fig. 3.5. Away from half-filling, the temperature is low enough that we may expect superfluidity, and thus enhanced c_{pair}-correlations; but *at* half-filling, the system does not order at finite temperature, there can be no superfluidity, and the LDA must see a decrease in c_{pair} around that point. The peak in c_{charge} does not come unexpected either, because at half-filling, the two correlations are proportional and develop long-range order at zero temperature; the elevated c_{charge} at $T > 0$ anticipates this transition.

The differing behavior of the trapped system is once again illuminated by a comparison with the repulsive model via the asymmetric particle-hole transformation (Sec. 2.3.2). Recall the following mappings under $ph_{\downarrow}$:

$$\begin{aligned} \text{chemical potential} &\leftrightarrow \text{magnetic field} \\ \text{s-wave pairing order} &\leftrightarrow \text{AF-}xy\text{ spin order}, \\ \text{double occupancy} &\leftrightarrow \text{spin-}\uparrow, \\ \text{empty site} &\leftrightarrow \text{spin-}\downarrow. \end{aligned}$$

In the repulsive picture, there is a large magnetic field at the edge of the system so that the spins there are frozen to $\downarrow$. Further inwards, at a moderate magnetic field, the spins are tilted out of the xy-plane (towards $\downarrow$ near the edge and $\uparrow$ near the center), but retain AF order in the xy-components.

In the LDA, we may imagine the spins at different radii disconnected. Thus the spins at half-filling, where the system is above the transition temperature, will not order. However, in the trapped system, the spins at half-filling are coupled the other regions, and this coupling forces xy order to continue through at half-filling.

The failure of the LDA in this case has implications for the quantum-simulator scheme. On the one hand, the observation of the superfluid phase in the AHM may be easier than expected in the LDA, because a larger portion of the system is in that phase.

On the other hand, observing the physics of the *half-filled* AHM in optical lattices is not straightforwardly possible, as that system is not properly represented anywhere in the trap. This is in contrast to the RHM, where the Mott plateau ensures that a half-filled region exists in the trap provided the density at the center is sufficiently large. Indeed, in the thermodynamic

limit, the half-filled annulus becomes truly two-dimensional in the RHM, whereas the half-filled region is only a one-dimensional ring in the AHM.

Recently, Ho et al. [25] suggested to emulate the *repulsive* Hubbard model with an optical lattice with *attractive* interactions, by inferring properties of the RHM via the asymmetric particle-hole transformation. The authors propose this method both for the half-filled and the doped RHM; the latter would be realized as a nonzero magnetization in the attractive emulator, i.e. a population imbalance between the states representing spin-$\uparrow$ and spin-$\downarrow$.

In the half-filled case, insofar as one is interested in the RHM at zero magnetic field, our findings pose a problem for this plan, because the zero-field case (i.e. half-filled in terms of the optical lattice) will not be represented in the trap. It is not clear to what extent this problem will persist for the doped RHM emulated by an attractive system with nonzero magnetization.

Off-diagonal confinement (ODC), as suggested by Rousseau et al. [50], is a supposable solution to the problem of absent half-filling. In ODC, the trap would be implemented as a spatially varying hopping t_i (experimentally, a spatial variation of laser intensity superimposed on the periodic variation that forms the lattice) which tends to zero as the edge of the system is approached, thus preventing the trapped atoms from leaving the system. In this case, regardless of the sign of the interaction, the system can be made uniformly half-filled.*

5.3 Statistical Fluctuations of c_{pair}

At low temperatures, statistical fluctuations appear in the estimator (4.16) for the correlation function c_{pair}. Fig. 5.4 shows time series to illustrate this behavior. The large variance of the signal results in unacceptably large statistical errors of the structure factor P_s. This represents a significant obstacle to studying the superfluid phase.

As these fluctuations appear in homogeneous as well as confined systems, we will return to the homogeneous case for the present discussion.

*In Ref. 50, it is demonstrated numerically for repulsive bosons in one dimension that $\hat{n}_i = 1$ for all sites in a certain bracket of chemical potential values. For our model, particle-hole symmetry implies $\hat{n}_i = 1$ at $\mu = 0$.

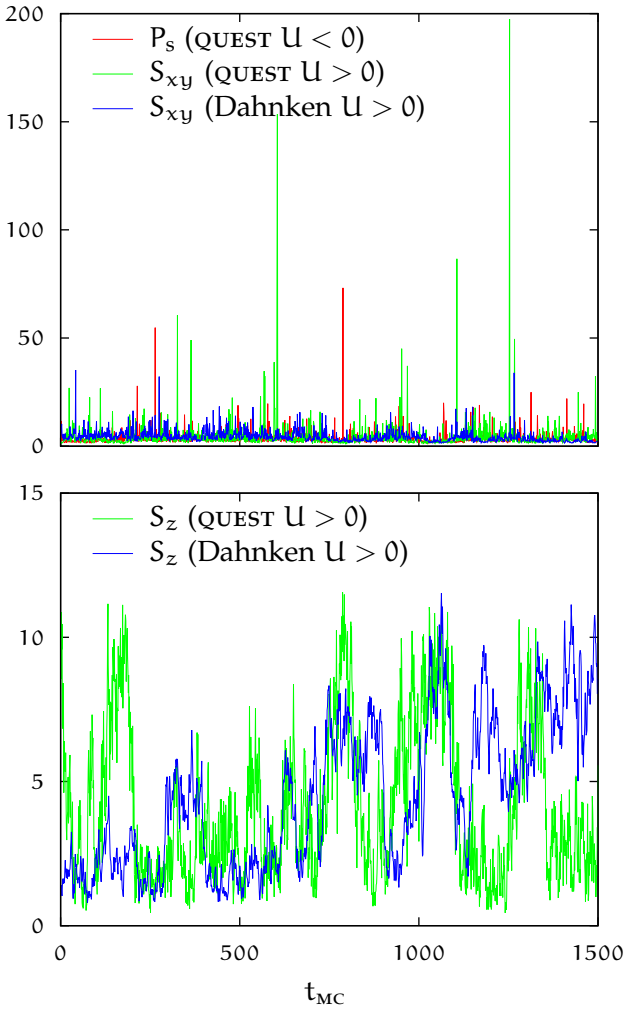

Figure 5.4: Time series of the problematic observables (top) and well-behaved observables (bottom) for comparison. The system is a homogeneous 4×4-lattice. Results from QUEST are compared to results obtained with Dahnken's DQMC code [15], and at the top, observables in the attractive model are compared to their equivalents in the repulsive case. Parameters: $\beta = 9\,t$, $|U| = 6\,t$ $\mu = h = 0$. The antiferromagnetic spin correlations in the xy-plane S_{xy} and in z-direction S_z are the repulsive-picture analogs of c_{pair} and c_{charge}, respectively. The Monte Carlo time t_{MC} is a counter of sweeps through the space-time lattice.

The problematic behavior appears already on systems as small as 4×4 at rather high temperatures ($T \lesssim 1/2\,t$), but becomes more pronounced as the temperature is lowered and the system enlarged. A weaker interaction ($U = -4\,t$) does not reduce the problem significantly.

Extensive tests were carried out to ensure that the outliers are *not* the result of numerical instabilities. Different approaches and parameters for numerical stabilization were tried within QUEST*, and results were compared to an independent implementation [15]. Different values for

the imaginary-time step were also compared. Finally, the repulsive model at $\mu = h = 0$ shows the same behavior as translated by the asymmetric particle-hole transformation $ph_\downarrow$. The z spin correlations are well-behaved, as is c_{charge} in the attractive picture; but the the xy spin correlations show the same problem as c_{pair} in the attractive picture.

5.3.1 Imaginary Hubbard-Stratonovich Transformation

A plausible remedy for the problem described above is suggested by Assaad's findings [2] on the spin correlation functions in the repulsive case. Using the SU(2)-symmetric Hubbard-Stratonovich transformation (4.9), and thus an imaginary λ, the xy spin fluctuations could be significantly improved at the expense of calculating with complex numbers.

Since the repulsive model with (4.9) is connected by the transformation $ph_\downarrow$ to the attractive model with (4.10) (which also implies an imaginary λ), it may be expected that a similar improvement is possible for the attractive model by switching to the alternate HST.

Note that Assaad's results are for $\mu = h = 0$. Thus, for $\mu \neq 0$ or even inhomogeneous μ as needed for the trap, no immediate conclusion is possible. On the other hand, in the AHM no essential difference in the c_{pair} fluctuations is seen between zero and nonzero μ. It is therefore reasonable to expect confined systems to benefit from the imaginary transformation as well.

At $h = 0$, the transformation (4.9) respects the SU(2) spin invariance of the model, as emphasized by Assaad; quantities related by a spin rotation have numerically equal estimators and the magnetization is zero for every HS field configuration [2], properties which for the alternative transformation (4.10) are only restored by the sum over all configurations. However, in the attractive case, while the model is still SU(2)-symmetric, it is the SU(2)-*un*symmetric transformation that is expected to provide

*First, using SVD decompositions to stabilize the product of the $\boldsymbol{B}$ matrices and the inversion leading to the Green's Function [3]. There are two parameters, which were also varied: The number of decompositions per product, and the number of times the Green's function is "wrapped" [39] before it is recomputed.

Second, using an $NM \times NM$ matrix which contains the $\boldsymbol{B}$ matrices instead of the string of $N \times N$ matrices [24]. This method is slower but considered more stable than the first.

improved estimator properties; what unites the two cases is that λ is imaginary.

At the time of this writing, the imaginary transformation was newly implemented in QUEST. Unfortunately, initial results show no improvement of the situation.

5.4 Phase Transition to a Superfluid Phase

The aim of this section is to investigate the low-temperature phase of the trapped AHM and the transition that separates it from the high-temperature phase. In analogy to the homogeneous model (see Sec. 2.4.2), the trapped model is expected to undergo a KT transition to a QLRO phase at low temperature. An FSS/TSS analysis as described in Sec. 2.5 (homogeneous case) and Sec. 3.3.1 (modifications for the confined case) can provide evidence for the trapped KT scenario if good agreement with the KT scaling behavior is found. In a study of the inhomogeneous classical xy-model, Crecchi and Vicari [14] have found evidence for a trapped KT transition using similar methodology.

While a conclusive FSS analysis in the scope of this study is frustrated by the difficulties outlined in the preceding section, we present a finite-size extrapolation (FSE) based on results for trapped systems with $L = 12, 14, \ldots, 24$ which points to a KT scenario with $T_c \sim 0.15\,t$. This section follows the discussion of Sec. 2.5 and presents the plots described there with the exception of the scaling plot of Fig. 2.4.

For comparison, an FSS for the homogeneous AHM is provided in Ref. 45, and some of the results are reproduced in Sec. 2.5. It should be pointed out that the results from Ref. 45 are for $U = -4\,t$ whereas ours are for $U = -6\,t$.

Fig. 5.5 shows the analog of Fig. 2.2 for the trapped case. At high temperatures, all systems sizes are equivalent because the correlation length is small in comparison to the system size. For lower temperatures, despite the noise, the curves are clearly seen to level off, showing a first sign of a transition to superfluidity.

Next, we address the question whether an "effective η'" as per (3.6) exists in Fig. 5.6. Indeed, our results are consistent with an exponential dependence of P_s on L. While an accurate determination of η' is impossible

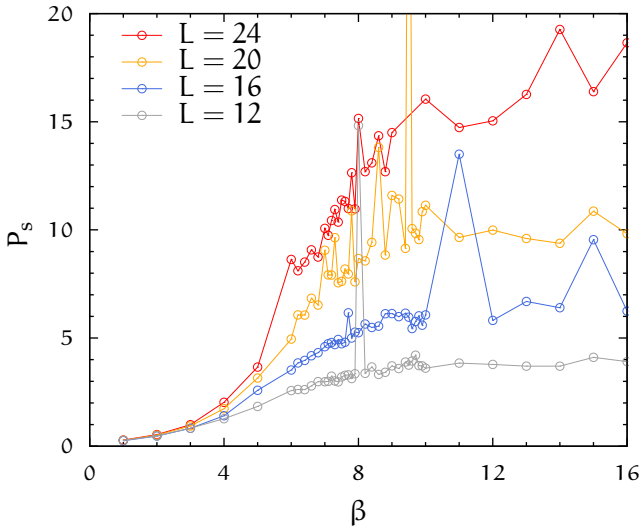

Figure 5.5: S-wave pairing structure factor P_s as a function of inverse temperature β for various system sizes L. At high temperature, where the correlation length is small, the results for all L coincide. As the correlation length grows, the curves separate. Eventually, they level off at low temperature to maximum values determined by L. This behavior is indicative of a phase transition.

β	T'	η'	$f(0)$	ζ
7.4	−0.10	0.197 ± 0.02	0.034 ± 0.002	0.179(1)
8.2	−0.19	0.119 ± 0.05	0.031 ± 0.005	
8.8	−0.24	0.115 ± 0.02	0.032 ± 0.002	
9.8	−0.32	0.122 ± 0.10	0.034 ± 0.01	
12	−0.44	-0.061 ± 0.14	0.020 ± 0.01	0.093(1)
13	−0.49	0.043 ± 0.13	0.028 ± 0.01	
15	−0.55	0.011 ± 0.06	0.029 ± 0.01	0.072(1)

Table 5.1: Results from the fits in Fig. 5.6, unrounded. Parameters were determined using a non-linear least-squares fit [57]. Because of excessive fluctuations in the s-wave measurement in DQMC, no accurate determination of the parameters is possible, but our results are compatible with an effective exponent η' in the size-dependence of the structure factor, see (2.10a) and (3.6) which is equal to the exponent in the homogeneous case. Reduced temperatures T' are calculated using $T_c = 0.15\,t$. Note that $\eta' < 0$ is an unphysical artifact of the least-squares fit. For comparison, we give results for the exponent ζ at equivalent reduced temperature from Ref. 14, which is identical to η' under the assumption (3.5).

with the present data, there is some indication of η' falling as temperature is lowered, as is expected for the KT transition.

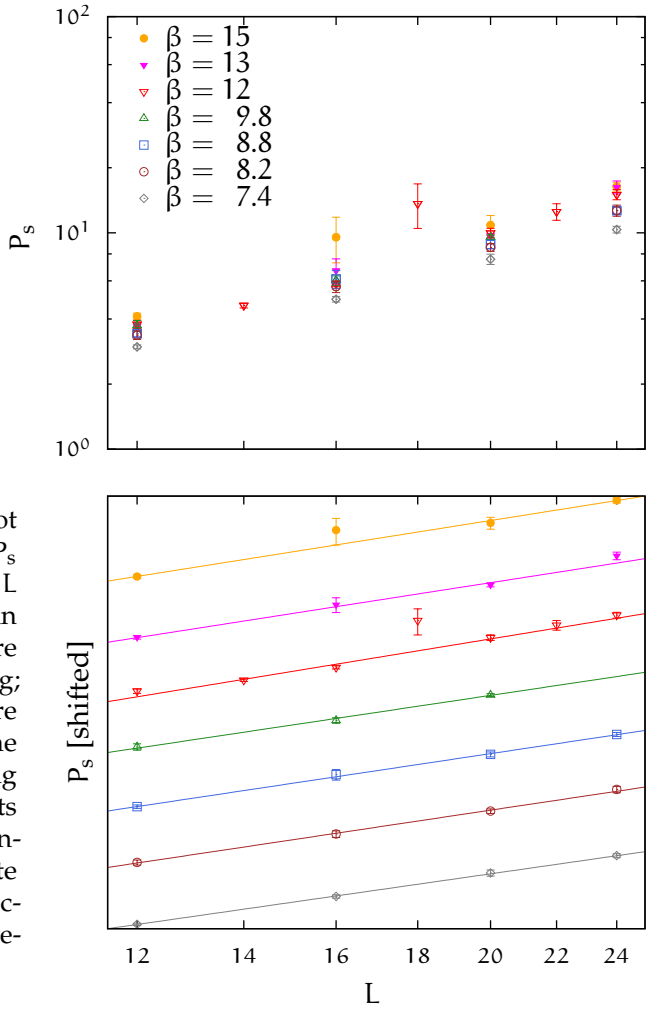

Figure 5.6: Doubly logarithmic plot of the s-wave structure factor P_s as a function of system size L for some of the temperatures in Fig. 5.5. At the top, the data are shown without further processing; at the bottom, the same points are shown with nonlinear fits of the form $P_s(L) = f(0)\, L^{2-\eta'}$ according to (3.6), and with constant offsets applied to make the curves distinguishable. Straight lines indicate the validity of (3.6) with an "effective exponent" η'. Numerical fit results are reported in Table 5.4.

This result may be compared to results of Ref. 14 where $\eta'(T) = \eta(T)$ is found for the classical xy-model, whose phase transition in the homogeneous case belongs to the same universality class. The results as reported in Table 5.4 appear compatible, although the large uncertainties for the AHM make interpretation difficult. The compatibility of the results evidently depends on the critical temperature T_c, which must be used to convert to reduced temperatures T', but accurate determination of T_c for the AHM was not possible.

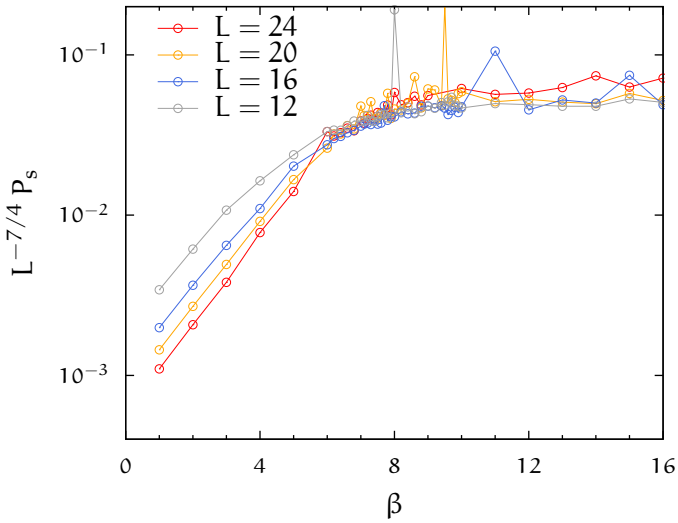

Figure 5.7: Logarithmic plot of the scaled s-wave structure factor P_s for various system sizes L as a function of inverse temperature β (error bars suppressed for clarity). Convergence of the curves at low temperature indicates a divergent correlation length and points to a KT transition. Within statistical errors, the results are compatible with a collapse around $\beta \sim 6 \ldots 8$, i.e. $T_c \sim 0.15\,t$. We have used $\eta' = .25$.

Finally, Fig. 5.7 shows the analog of Fig. 2.3 for the confined system using $\eta' = .25$. Within statistical errors, the curves are observed to converge at low temperature, again consistent with a KT transition in the confined system. This figure also provides the best means at our disposal to determine the transition temperature T_c. The collapse of the curves occurs around $T_c \sim 0.15\,t$, which should be taken as a rough estimate. This value is similar to values found for the homogeneous system across a wide range of fillings [45].

In summary, within the statistical uncertainties, all signs point toward a KT transition in the trap at a critical temperature similar to the homogeneous case. From Figs. 5.5 and 5.7, we can conclude with some confidence that the correlation length diverges for large systems when the trapping potential is made weaker as the system size increases in accordance with (3.4). Fig. 5.6 and Table 5.4 are consistent with the scaling behavior (3.6), which would indicate that the transition is indeed of KT-type.

6 Conclusion

The focus of this work was the attractive Fermi-Hubbard model in a confining potential, in particular the quasi-long-range-ordered superfluid phase that occurs at low temperatures away from half-filling (i.e., one particle per site). Interest in this model is motivated by experiments on ultra-cold quantum gases in optical lattices, which can be made to emulate the Hubbard model with repulsive or attractive interactions.

Superconductivity is more easily studied when the interaction between the particles is attractive, because the fermion sign problem of quantum Monte Carlo simulations can be circumvented in that case, and because the temperature scale for superfluidity is higher than that for superconductivity in the repulsive case, which is only putative in any event.

Two ideas served to guide the discussion of the model, both of which are at once convenient technical tools and conceptually interesting in their own right. First, two related *particle-hole transformations* were introduced, which provide exact mappings between different parameter regimes of the Fermi-Hubbard model; in one case, the sign of the chemical potential is reversed, thus densities above half-filling are mapped to below half-filling; in the other case, it is the interaction that changes sign, providing a relation between the attractive and the repulsive Hubbard model. These transformations are equally valid for the homogeneous case as for the trapped case, where they can be understood to act locally on each site.

Second, the local-density approximation (LDA) connects the confined model to the homogeneous case by replacing each site in the inhomogeneous lattice with results from the homogeneous model. We argued that the validity of this procedure is crucial for the *quantum-simulator* program, which aims to translate observations of confined systems into a deeper understanding of the corresponding homogeneous systems.

A general prediction of the LDA is that different phases of the homogeneous model may coexist in one confined system, because the phase depends on the particle density, which becomes inhomogeneous in the

trap. For the repulsive Hubbard model, this coexistence is already visible in the radial density profile where flat regions, i.e. a vanishing local compressibility, indicate a Mott-insulating phase. In the attractive case, no such "Mott plateaux" appear. The LDA and simulations of true confined systems agree on this point, a simple argument based on the sign of the energy associated with a shared site provides an intuitive explanation. Nevertheless, a coexistence of superfluid and normal regions is expected at sufficiently low temperatures.

In the literature, the LDA has been found to be accurate in most cases, except where the density in the trap varies abruptly, such as at the edges of a Mott plateau in the confined repulsive Hubbard model.

In the case of the attractive Hubbard model, our findings indicate a *qualitative failure of the* LDA around half-filling. This may be understood using the homogeneous-case phase diagram; at half-filling, the s-wave-pairing and charge-density-wave correlations are degenerate, which leads to the transition temperature being suppressed to zero. The LDA sees this in full and predicts sharp features in both correlation functions at the half-filled point; however, in the true confined system, these features are washed out by the coupling to regions of different density. The latter mechanism is illuminated by the asymmetric particle-hole transformation, which maps the pairing to spin order.

The implications of this result are twofold. On the one hand, observation of superfluidity in an attractive optical lattice is simplified, because a larger portion of the system may be expected to be superfluid. On the other hand, observation of the physics of the *half-filled* attractive Hubbard model in optical lattices is impeded, because that physics is not properly represented anywhere in the trap. Whereas in the repulsive case, thanks to the Mott gap, a half-filled region exists which becomes truly two-dimensional in the thermodynamic limit; in the attractive case, there is only a one-dimensional ring of half-filling. We argued the proposed technique of *off-diagonal confinement*, if realized experimentally, would remedy this situation.

To shed light on the low-temperature phase of the confined attractive Hubbard model, a scaling analysis was made. A Kosterlitz-Thouless transition is expected in analogy to the homogeneous case. We reviewed the scaling procedure for this transition type and the differences that arise as a result of the trap, and presented results from a series of system sizes in

accordance with the resulting "trap-size scaling" procedure.

However, a complete finite-size scaling was hampered by excessive fluctuations in the estimator for the pairing correlations, resulting in large statistical errors. To the extent that a finite-size extrapolation was possible with the data available, we find results compatible with the expected Kosterlitz-Thouless transition to a quasi-long-range-ordered superfluid state with a transition temperature around $T_c \sim 0.15\,t$, similar to the values found for the homogeneous system over a wide range of particle density.

Bibliography

[1] P. W. Anderson. The resonating valence bond state in La_2CuO_4 and superconductivity. *Science*, 235(4793):1196 –1198, Mar. 1987. Cited on page 17.

[2] F. F. Assaad. SU(2)-spin invariant auxiliary field quantum Monte Carlo algorithm for Hubbard models. In E. Krause and W. Jäger, editors, *High performance computing in science and engineering*. Springer, Berlin, Heidelberg, New-York, 1998. Cited on pages 45 and 59.

[3] Z. Bai, W. Chen, R. T. Scalettar, and I. Yamazaki. Numerical methods for quantum Monte Carlo simulations of the Hubbard model, Feb. 2008. Cited on pages 49 and 59.

[4] W. S. Bakr, J. I. Gillen, A. Peng, S. Folling, and M. Greiner. A quantum gas microscope for detecting single atoms in a Hubbard-regime optical lattice. *Nature*, 462(7269):74–77, Nov. 2009. Cited on page 31.

[5] G. G. Batrouni, V. Rousseau, R. T. Scalettar, M. Rigol, A. Muramatsu, P. J. H. Denteneer, and M. Troyer. Mott domains of bosons confined on optical lattices. *Physical Review Letters*, 89(11):117203, 2002. Cited on page 38.

[6] G. G. Batrouni and R. T. Scalettar. Anomalous decouplings and the fermion sign problem. *Physical Review B*, 42(4):2282, 1990. Cited on page 50.

[7] V. L. Berezinskiı. Breaking of long–range ordering in one–and two–dimensional systems with continious symmetry group. *Sov. Phys JETP*, 34:610, 1972. Cited on page 24.

[8] R. Blankenbecler, D. J. Scalapino, and R. L. Sugar. Monte Carlo calculations of coupled boson-fermion systems. *Physical Review D*, 24(8):2278, Oct. 1981. Cited on page 42.

[9] I. Bloch. Quantum gases in optical lattices. *Physics World*, 17(4):25–29, Apr. 2004. Cited on page 13.

[10] M. Campostrini and E. Vicari. Critical behavior and scaling in trapped systems. *Physical Review Letters*, 102(24):240601, June 2009. Cited on page 36.

[11] S. Chiesa, C. N. Varney, M. Rigol, and R. T. Scalettar. Magnetism and pairing of two-dimensional trapped fermions. *Physical Review Letters*, 106(3):035301, Jan. 2011. Cited on page 39.

[12] C. Chin, R. Grimm, P. Julienne, and E. Tiesinga. Feshbach resonances in ultracold gases. *Reviews of Modern Physics*, 82(2):1225, Apr. 2010. Cited on page 30.

[13] J. D. Cone, A. Zujev, and R. T. Scalettar. Isentropic curves at magnetic phase transitions. *Physical Review B*, 83(4):045108, Jan. 2011. Cited on page 32.

[14] F. Crecchi and E. Vicari. Quasi-long-range order in trapped systems. *Physical Review A*, 83(3):035602, Mar. 2011. Cited on pages 36, 60, 61, and 62.

[15] C. Dahnken. *Elektronische Anregungen des Hubbard-Modells mit langreichweitiger Wechselwirkung*. Diploma thesis, Bayerische Julius-Maximiliam-Universität, Würzburg, 1998. Cited on pages 51 and 58.

[16] V. J. Emery. Theory of the quasi-one-dimensional electron gas with strong "on-site" interactions. *Physical Review B*, 14(7):2989, Oct. 1976. Cited on page 22.

[17] T. Esslinger. Fermi-Hubbard physics with atoms in an optical lattice. *arXiv:1007.0012v1*, June 2010. Cited on page 29.

[18] H. G. Evertz. Analytische Behandlung von Vielteilchenproblemen: Hubbard- und Heisenbergmodell, 2004. Lecture notes. Cited on page 23.

[19] P. Fazekas. *Lecture Notes on Electron Correlation and Magnetism*. World Scientific, Singapore, 1999. Cited on page 17.

[20] M. P. A. Fisher, P. B. Weichman, G. Grinstein, and D. S. Fisher. Boson localization and the superfluid-insulator transition. *Physical Review B*, 40(1):546, July 1989. Cited on pages 37 and 38.

[21] M. Greiner, O. Mandel, T. Esslinger, T. W. Hansch, and I. Bloch. Quantum phase transition from a superfluid to a Mott insulator in a gas of ultracold atoms. *Nature*, 415(6867):39–44, Jan. 2002. Cited on pages 13, 29, and 37.

[22] J. E. Hirsch. Discrete Hubbard-Stratonovich transformation for fermion lattice models. *Physical Review B*, 28(7):4059, Oct. 1983. Cited on page 42.

[23] J. E. Hirsch. Two-dimensional Hubbard model: Numerical simulation study. *Physical Review B*, 31(7):4403, Apr. 1985. Cited on page 51.

[24] J. E. Hirsch. Stable Monte Carlo algorithm for fermion lattice systems at low temperatures. *Physical Review B*, 38(16):12023, Dec. 1988. Cited on page 59.

[25] A. F. Ho, M. A. Cazalilla, and T. Giamarchi. Quantum simulation of the Hubbard model: the attractive route. *Physical Review A*, 79(3):033620, Mar. 2009. Cited on pages 39 and 57.

[26] J. Hubbard. Calculation of partition functions. *Physical Review Letters*, 3(2):77, July 1959. Cited on page 42.

[27] J. Hubbard. Electron correlations in narrow energy bands. *Proceedings of the Royal Society of London. Series A. Mathematical and Physical Sciences*, 276(1365):238 –257, Nov. 1963. Cited on page 17.

[28] D. Jaksch. Optical lattices, ultracold atoms and quantum information processing. *quant-ph/0407048*, July 2004. Cited on page 29.

[29] D. Jaksch, C. Bruder, J. I. Cirac, C. W. Gardiner, and P. Zoller. Cold bosonic atoms in optical lattices. *Physical Review Letters*, 81(15):3108, Oct. 1998. Cited on pages 13, 29, 30, and 37.

[30] R. Jördens, L. Tarruell, D. Greif, T. Uehlinger, N. Strohmaier, H. Moritz, T. Esslinger, L. D. Leo, C. Kollath, A. Georges, V. Scarola, L. Pollet,

E. Burovski, E. Kozik, and M. Troyer. Quantitative determination of temperature in the approach to magnetic order of ultracold fermions in an optical lattice. *Physical Review Letters*, 104(18):180401, May 2010. Cited on page 32.

[31] A. Koga, T. Higashiyama, K. Inaba, S. Suga, and N. Kawakami. Supersolid state in a fermionic optical lattice system. *Journal of Physics: Conference Series*, 150(3):032046, Feb. 2009. Cited on page 53.

[32] M. Köhl, H. Moritz, T. Stöferle, K. Günter, and T. Esslinger. Fermionic atoms in a three dimensional optical lattice: Observing Fermi surfaces, dynamics, and interactions. *Physical Review Letters*, 94(8):080403, Mar. 2005. Cited on page 13.

[33] J. M. Kosterlitz. The critical properties of the two-dimensional XY model. *Journal of Physics C: Solid State Physics*, 7:1046, 1974. Cited on page 24.

[34] J. M. Kosterlitz and D. J. Thouless. Ordering, metastability and phase transitions in two-dimensional systems. *Journal of Physics C: Solid State Physics*, 6:1181, 1973. Cited on page 24.

[35] C. R. Lee, Z. Bai, R. Scalettar, M. Jarrell, S. Chiesa, C. Varney, W. Chen, I. Yamazaki, E. D'Azevedo, S. Savrasov, et al. *QUEST: Quantum Electron Simulation Toolbox*. 2008. Cited on page 51.

[36] M. Lewenstein, A. Sanpera, V. Ahufinger, B. Damski, A. S. De, and U. Sen. Ultracold atomic gases in optical lattices: Mimicking condensed matter physics and beyond. *Advances in Physics*, 56(1-2):243–379, 2007. Cited on pages 13 and 29.

[37] E. Lieb. The Hubbard Model: Some rigorous results and open problems. *XI Int. Cong. MP, Int. Press*, pages 392–412, 1995. XI Int. Cong. MP, Int. Press (1995) 392-412. Cited on page 17.

[38] E. Y. Loh, J. E. Gubernatis, R. T. Scalettar, S. R. White, D. J. Scalapino, and R. L. Sugar. Sign problem in the numerical simulation of many-electron systems. *Physical Review B*, 41(13):9301, May 1990. Cited on page 50.

[39] E. Y. J. Loh and J. E. Gubernatis. Stable numerical simulations of models of interacting electrons in condensed-matter physics. In W. Hanke and Y. Kopaev, editors, *Electronic Phase Transitions*. Elsevier, New York, 1992. Cited on pages 42, 46, 48, 49, and 59.

[40] K. W. Mahmud, E. N. Duchon, Y. Kato, N. Kawashima, R. T. Scalettar, and N. Trivedi. Finite temperature study of bosons in a two dimensional optical lattice. *arXiv:1101.5726v1*, Jan. 2011. Cited on pages 37 and 38.

[41] N. D. Mermin and H. Wagner. Absence of ferromagnetism or antiferromagnetism in one- or two-dimensional isotropic Heisenberg models. *Physical Review Letters*, 17(22):1133, Nov. 1966. Cited on pages 23 and 33.

[42] A. Moreo and D. J. Scalapino. Two-dimensional negative-U hubbard model. *Physical Review Letters*, 66(7):946, Feb. 1991. Cited on page 25.

[43] W. J. Mullin. Bose-Einstein condensation in a harmonic potential. *Journal of Low Temperature Physics*, 106(5-6):615–641, 1997. Cited on pages 33 and 34.

[44] P. Olsson. Monte Carlo analysis of the two-dimensional XY model. II. comparison with the kosterlitz renormalization-group equations. *Physical Review B*, 52(6):4526, 1995. Cited on pages 24 and 36.

[45] T. Paiva, R. R. dos Santos, R. T. Scalettar, and P. J. H. Denteneer. Critical temperature for the two-dimensional attractive Hubbard model. *Physical Review B*, 69(18):184501, May 2004. Cited on pages 25, 26, 27, 40, 60, and 63.

[46] R. Peierls. Zur Theorie des Diamagnetismus von Leitungselektronen. *Zeitschrift für Physik*, 80(11-12):763–791, 1933. Cited on page 18.

[47] M. Rigol, G. G. Batrouni, V. G. Rousseau, and R. T. Scalettar. State diagrams for harmonically trapped bosons in optical lattices. *Physical Review A*, 79(5):053605, May 2009. Cited on page 34.

[48] M. Rigol and A. Muramatsu. Quantum Monte Carlo study of confined fermions in one-dimensional optical lattices. *Physical Review A*, 69(5):053612, May 2004.

[49] M. Rigol, A. Muramatsu, G. G. Batrouni, and R. T. Scalettar. Local quantum criticality in confined fermions on optical lattices. *Physical Review Letters*, 91(13):130403, 2003. Cited on page 34.

[50] V. G. Rousseau, G. G. Batrouni, D. E. Sheehy, J. Moreno, and M. Jarrell. Pure Mott phases in confined ultracold atomic systems. *Physical Review Letters*, 104(16):167201, Apr. 2010. Cited on pages 51 and 57.

[51] R. T. Scalettar, E. Y. Loh, J. E. Gubernatis, A. Moreo, S. R. White, D. J. Scalapino, R. L. Sugar, and E. Dagotto. Phase diagram of the two-dimensional negative-U Hubbard model. *Physical Review Letters*, 62(12):1407, Mar. 1989. Cited on page 23.

[52] T. Schneider and J. M. Singer. *Phase Transition Approach to High-Temperature Superconductivity*, volume 17. Imperial College Press, 2000. Cited on pages 17 and 19.

[53] R. L. Stratonovich. On a method of calculating quantum distribution functions. *Soviet Physics Doklady*, 2:416, July 1957. Cited on page 42.

[54] M. Suzuki. Generalized trotter's formula and systematic approximants of exponential operators and inner derivations with applications to many-body problems. *Communications in Mathematical Physics*, 51(2):183–190, 1976. Cited on page 44.

[55] W. von der Linden. A quantum Monte Carlo approach to many-body physics. *Physics Reports*, 220(2-3):53–162, 1992. Cited on pages 42 and 48.

[56] S. R. White, D. J. Scalapino, R. L. Sugar, E. Y. Loh, J. E. Gubernatis, and R. T. Scalettar. Numerical study of the two-dimensional Hubbard model. *Physical Review B*, 40(1):506, July 1989. Cited on page 23.

[57] T. Williams and C. Kelley. Gnuplot 4.4. `http://www.gnuplot.info/docs_4.4/gnuplot.pdf`, Mar. 2010. Cited on page 61.